

This discussion paper is/has been under review for the journal Atmospheric Chemistry and Physics (ACP). Please refer to the corresponding final paper in ACP if available.

Potential of polarization lidar to provide profiles of CCN- and INP-relevant aerosol parameters

R. E. Mamouri¹ and A. Ansmann²

¹Cyprus University of Technology, Dep. of Civil Engineering and Geomatics, Limassol, Cyprus

²Leibniz Institute for Tropospheric Research, Leipzig, Germany

Received: 30 October 2015 – Accepted: 16 November 2015 – Published: 4 December 2015

Correspondence to: R. E. Mamouri (rodanthi.mamouri@cut.ac.cy)

Published by Copernicus Publications on behalf of the European Geosciences Union.

ACPD

15, 34149–34204, 2015

Lidar profiling of
CCN- and
INP-relevant aerosol
parameters

R. E. Mamouri and
A. Ansmann

Title Page	
Abstract	Introduction
Conclusions	References
Tables	Figures
 ◀	 ▶
 ◀	 ▶
Back	Close
Full Screen / Esc	
Printer-friendly Version	
Interactive Discussion	

Abstract

We investigate the potential of polarization lidar to provide vertical profiles of aerosol parameters from which cloud condensation nucleus (CCN) and ice nucleating particle (INP) number concentrations can be estimated. We show that height profiles of number concentrations of aerosol particles with radius $> 50\text{ nm}$ (APC_{50} , reservoir of favorable CCN) and with radius $> 250\text{ nm}$ (APC_{250} , reservoir of favorable INP), as well as profiles of the aerosol particle surface area concentration (ASC, used in INP parameterization) can be retrieved from lidar-derived aerosol extinction coefficients (AEC) with relative uncertainties of a factor of around 2 (APC_{50}), and of about 25–50 % (APC_{250} , ASC).
5 Of key importance is the potential of polarization lidar to identify mineral dust particles and to distinguish and separate the aerosol properties of basic aerosol types such as mineral dust and continental pollution (haze, smoke). We investigate the relationship between AEC and APC_{50} , APC_{250} , and ASC for the main lidar wavelengths of 355, 532 and 1064 nm and main aerosol types (dust, pollution, marine). Our study is based on
10 15 multiyear Aerosol Robotic Network (AERONET) photometer observations of aerosol optical thickness and column-integrated particle size distribution at Leipzig, Germany, and Limassol, Cyprus, which cover all realistic aerosol mixtures of continental pollution, mineral dust, and marine aerosol. We further include AERONET data from field campaigns in Morocco, Cabo Verde, and Barbados, which provide pure dust and pure
15 20 marine aerosol scenarios. By means of a simple relationship between APC_{50} and the CCN-reservoir particles (APC_{CCN}) and published INP parameterization schemes (with APC_{250} and ASC as input) we finally compute APC_{CCN} and INP concentration profiles. We apply the full methodology to a lidar observation of a heavy dust outbreak crossing Cyprus with dust up to 8 km height and to a case during which anthropogenic pollution dominated.
25

Lidar profiling of CCN- and INP-relevant aerosol parameters

R. E. Mamouri and
A. Ansmann

[Title Page](#)

[Abstract](#)

[Introduction](#)

[Conclusions](#)

[References](#)

[Tables](#)

[Figures](#)

[|◀](#)

[▶|](#)

[◀](#)

[▶](#)

[Back](#)

[Close](#)

[Full Screen / Esc](#)

[Printer-friendly Version](#)

[Interactive Discussion](#)



1 Introduction

Field studies of aerosol-cloud-dynamics interaction are presently in the focus of atmospheric research. Large uncertainties in weather and future-climate predictions (IPCC, 2013) arise from gaps in our knowledge of the detailed impact of aerosols on the evolution of liquid-water, mixed-phase and cirrus clouds. This unsatisfactory situation motivates the strong efforts presently undertaken to investigate formation and evolution of cloud layers and associated aerosol-cloud interactions.

Aerosol particles influence cloud evolution, lifetime, and cloud microphysical properties in two ways. Aerosol particles can serve as cloud condensation nuclei (CCN) in liquid droplet nucleation processes and/or as ice-nucleating particles (INP) in ice crystal nucleation processes which include also the conversion of liquid droplets into ice crystals (immersion freezing). Ground-based active remote sensing (lidar and radar observations) is requested to continuously monitor the evolution of clouds in their natural environment, at given meteorological conditions with high vertical and temporal resolution (Illingworth et al., 2007; Shupe, 2007; Ansmann et al., 2009; de Boer et al., 2011; Schmidt et al., 2014).

Lidar is the most prominent tool for aerosol profiling in terms of particle optical properties. However, to improve the study of aerosol-cloud interaction, the potential of lidar to provide vertical profiles of the number concentration of particles with radius $> 30\text{--}50\text{ nm}$ ($\text{APC}_{30}\text{--}\text{APC}_{50}$, main reservoir of favorable particles that can act as CCN, in the following denoted as APC_{CCN}) (Quinn et al., 2008; Rose et al., 2010; Deng et al., 2011) and particles with radius $> 250\text{ nm}$ (APC_{250} , reservoir of favorable INP) (DeMott et al., 2010, 2015) as well as of the particle surface area concentration (ASC, a proxy for the ice nucleation active surface sites) (Niemand et al., 2012; Steinke et al., 2015) needs to be explored in detail.

The central question of our study is: Can we use lidar-derived vertical profiles of aerosol backscatter and extinction coefficients (AEC) to estimate vertical profiles of APC_{30} , APC_{50} , APC_{250} , and ASC from which the cloud-relevant APC_{CCN} and INP con-

Title Page

Abstract

Introduction

Conclusions

References

Tables

Figures

◀

▶

Back

Close

Full Screen / Esc

Printer-friendly Version

Interactive Discussion

centration (INPC) profiles can be estimated? A first promising feasibility study regarding the retrieval of INPC profiles from lidar observations was undertaken by Mamouri and Ansmann (2015). Former studies indicate also that measured aerosol optical properties (at wavelengths around 500 nm) can be used to estimate CCN concentration (CCNC) (Ghan and Collins, 2004; Ghan et al., 2006; Andreae, 2009; Jefferson, 2010; Liu and Li, 2014; Shinozuka et al., 2015). Complicating aspects arise however from the fact that optically active aerosol particles for typical lidar wavelengths of 355–1064 nm have radii $> 40\text{--}50$ nm and thus the derivable APC_{50} does not fully cover the entire CCN-relevant aerosol sizes.

A crucial point regarding INPC profiling is that the efficacy of aerosol particles to serve as ice nuclei depends on the aerosol type. It is found that mineral dust particles are fully activated at temperatures below about -20°C (Ansmann et al., 2009; Murray et al., 2012; Augustin-Bauditz et al., 2014), that marine particles seem to be comparably inefficient INPs (Kanitz et al., 2011) at temperatures $> -25^\circ\text{C}$, whereas continental particle mixtures (mixtures of anthropogenic haze, biomass burning smoke, soil and road dust, and biogenic particles) seem to contain always a significant amount of efficient INPs, already leading to ice nucleation at temperatures as high as -5 to -15°C (Seifert et al., 2010; Zhang et al., 2010; Kamphus et al., 2010; Ebert et al., 2011; Augustin et al., 2013; Hartmann et al., 2013; Bühl et al., 2013; Pummer et al., 2015; Umo et al., 2015). Thus, lidar must be able to separate these basic aerosol types and to provide APC_{CCN} and INPC profiles separately for marine, pollution, and dust particles.

In principle, multiwavelength Raman/polarization or high-spectral-resolution (HSR)/polarization lidars can provide the desired microphysical particle properties (Müller et al., 2005; Veselovskii et al., 2010; Müller et al., 2013, 2014). However comparably complex lidars and comprehensive data analysis methods as well as a good knowledge in the use of ill-posed inversion techniques are required to make these efforts successful. For this reason, we investigate an alternative approach. The overall goal is to develop a robust and easy-to-apply method that allows fast computation and implementation of an automated code in the lidar aerosol and

Lidar profiling of CCN- and INP-relevant aerosol parameters

R. E. Mamouri and
A. Ansmann

[Title Page](#)

[Abstract](#)

[Introduction](#)

[Conclusions](#)

[References](#)

[Tables](#)

[Figures](#)

◀

▶

[Back](#)

[Close](#)

[Full Screen / Esc](#)

[Printer-friendly Version](#)

[Interactive Discussion](#)



cloud data analysis software. Thus, the method should be simple and applicable to single-wavelength lidar observations at 355, 532, or 1064 nm wavelength to retrieve estimated profiles of APC_{50} , APC_{250} , and ASC. Many lidars are single-wavelength lidars (e.g., 355 or 532 nm backscatter lidars) including the upcoming space lidars of the European Space Agency operating at 355 nm (Ansmann et al., 2007; Illingworth et al., 2015) which are planned to be launched within the next 2–3 years. Furthermore, a dense European single-wavelength ceilometer network is developing, organized by European weather services (<http://www.dwd.de/ceilomap>) (Wiegner and Geiß, 2012; Wiegner et al., 2014).

However, to make full use of the retrieval schemes presented in this article, polarization lidars (Freudenthaler et al., 2009) are of advantage. This is a key point of the entire study. By means of the polarization lidar technique, dust and non-dust contributions to the measured particle optical properties can be separated. As will be shown, the aerosol properties, including the ones which are relevant for liquid-water cloud and mixed-phase cloud formation, can be separately determined for the basic aerosol types (mineral dust, marine aerosol, anthropogenic haze and smoke mixtures).

The following study is based on our long experience in detection, separation, and quantification of optical and microphysical properties of different aerosol types by using polarization lidars in combination with sun photometers (Tesche et al., 2009, 2011; Ansmann et al., 2011b, 2012; Mamouri et al., 2013; Mamouri and Ansmann, 2014; Nisantzi et al., 2014, 2015). The study presented here can be regarded as a follow-up effort of Mamouri and Ansmann (2015). However, in a much broader and more general sense, we now illuminate the potential of lidar to provide cloud-formation-relevant aerosol parameters for both liquid-water droplet and ice crystal nucleation. New aspects deal with the estimation of APC_{50} and ASC from measured optical properties and the consideration of INP parameterizations developed by Niemand et al. (2012) and Steinke et al. (2015), in which the particle surface area concentration ASC instead of APC_{250} is an input parameter. Furthermore, in the present study the wavelength range is extended from 532 nm to all three relevant laser wavelengths so that the CCN

[Title Page](#)[Abstract](#)[Introduction](#)[Conclusions](#)[References](#)[Tables](#)[Figures](#)[|◀](#)[▶|](#)[◀](#)[▶](#)[Back](#)[Close](#)[Full Screen / Esc](#)[Printer-friendly Version](#)[Interactive Discussion](#)

and INP-relevant aerosol conversion parameters are available for 355 and 1064 nm as well. We provide the wavelength-resolved conversion parameters for the mentioned aerosol types of mineral dust, maritime aerosol, continental pollution.

The study makes use of multiyear photometer observations of the Aerosol Robotic Network (AERONET) (Holben et al., 1998). Fourteen years of observations at Leipzig, Germany, 4 years at Limassol, Cyprus, and 7.5 years at Ragged Point, Barbados, are available. We further include AERONET data from mineral dust field campaigns at Morocco, Cabo Verde, and Barbados. The main reason to use AERONET observations (rather than performing a simulation study) is that we want to investigate the link between the optical and microphysical aerosol properties for “real-world” aerosol conditions. Long-term AERONET observations reflect best the full range of occurring aerosol mixture and layering scenarios. An alternative approach would be an extended simulation study similar to the study presented by Barnaba and Gobbi (2001) for marine and dust aerosols.

The paper is organized as follows: The AERONET stations and measurement products as well as the lidar sites and lidar products are given in Sect. 2. Section 3 presents our methodology to obtain profiles of APC_{50} , APC_{250} , ASC, APC_{CCN} , and INPC from lidar profiles of particle extinction coefficients AEC. In this approach, numerous conversion parameters are required. These parameters are obtained from the extensive AERONET data analysis (with focus on the correlations between aerosol optical depth at 355, 532, and 1064 nm and column values of APC_{50} , APC_{250} , and ASC). The main findings of this study are presented and discussed in Sect. 4. Section 5 finally deals with the application of the developed methods to two lidar observations conducted (a) during a strong dust outbreak towards Cyprus and (b) during conditions with dominating fine-mode pollution particles over Cyprus. A summary and concluding remarks are given in Sect. 6.

Title Page

Abstract

Introduction

Conclusions

References

Tables

Figures

|◀

▶|

◀

▶|

Back

Close

Full Screen / Esc

Printer-friendly Version

Interactive Discussion

2 Instrumentation

In Sect. 2.1, we provide an overview of the AERONET stations and the basic computations of APC_{50} , APC_{250} , and ASC as well as of AOT (aerosol particle optical thickness) for the specific lidar wavelengths at 355, 532, and 1064 nm. In Sect. 2.2, we briefly describe our lidar instruments.

2.1 AERONET sun/sky photometers

The study is based on the analysis of 3 long-term and 4 field-campaign Aerosol Robotic Network (AERONET) observational data sets. AERONET provides quality-assured product in terms of AOT at up to 8 wavelengths (340 to 1640 nm), and column-integrated values for the Ångström exponent (AE, spectral dependence of AOT), particle effective radius, volume concentration, surface area (column ASC), and particle size distribution, from which column-integrated APC_{50} and APC_{250} values can be computed. We investigated 14 years of AERONET observations at Leipzig, Germany, performed by the Leibniz Institute for Tropospheric Research (TROPOS). Leipzig is a highly polluted central European city which is affected by Saharan dust outbreaks about 2–10 times per year (Mattis et al., 2004, 2008). We analyzed 4 years of AERONET observations at Limassol, Cyprus, performed by the Cyprus University of Technology (CUT). This site in the eastern Mediterranean is a unique station for aerosol studies. Aerosol mixtures of anthropogenic haze, biomass burning smoke, soil dust, and marine particles, and strong dust outbreaks from Middle East deserts and the Sahara frequently occur (Nisantzi et al., 2015). Our studies are complimented by AERONET observations conducted during the Saharan Mineral Dust Experiments SAMUM-1 (Ouarzazate, Morocco) (Toledano et al., 2009) and SAMUM-2 (Praia, Cabo Verde) (Toledano et al., 2011; Ansmann et al., 2011a), the Saharan Aerosol Long-range Transport and Aerosol-Cloud interaction Experiments SALTRACE-1 (at the Caribbean Institute for Meteorology and Hydrology (CIMH), Barbados, summer 2013) and during SALTRACE-3 (Barbados, summer 2014) (Ansmann et al., 2014). The field campaigns offer the unique

Title Page

Abstract

Introduction

Conclusions

References

Tables

Figures

|◀

▶|

◀

▶

Back

Close

Full Screen / Esc

Printer-friendly Version

Interactive Discussion



opportunity to study the link between the particle optical properties (AEC, AOT) and the microphysical properties (APC_{50} , APC_{250} , ASC) at pure dust conditions. For the field campaigns, day-by-day multiwavelength Raman/polarization lidar observations of dust layer base and top heights and internal layering structures are available (Tesche et al., 2009, 2011; Haarig et al., 2015; Groß et al., 2015). Furthermore, we used the data from the AERONET station at Ragged Point, Barbados (level 2.0, 2007–2015) (Prospero and Mayol-Bracero, 2013) to study the link between the optical and microphysical aerosol properties for pure marine conditions.

An overview of the observational periods and amount of available data for the analyzed different aerosol conditions with focus on the three defined aerosol types are given in Table 1. More details of these AERONET stations can be found on the AERONET web page (<http://aeronet.gsfc.nasa.gov>) and in the publications of Toledano et al. (2009, 2011), Mamouri and Ansmann (2014), Nisantzi et al. (2015), and Prospero and Mayol-Bracero (2013).

The AERONET photometers deliver AOT values at up to 8 wavelengths from 340–1640 nm. Sky radiance observations are taken at 4 wavelengths. From these measurements the column-integrated particle size distribution is retrieved (Dubovik and King, 2000; Dubovik et al., 2006). In Sect. 4, we will study the relationships between column-integrated APC_{50} , APC_{250} , and ASC values and AOT for 355, 532, and 1064 nm. AERONET provides AOTs for 340, 380, 440, 500, 675, 870, 1020, and 1640 nm, so that AOTs at the laser wavelengths of 355, 532 and 1064 nm are obtained by inter and extrapolation. In the case of 355 nm we use the measured AOT at 380 nm and the Ångström exponent AE (340–380 nm) for this wavelength range. Similarly, in the case of 532 nm we use the measured AOT at 500 and AE (440–870 nm). The AOT at 1064 nm is obtained by extrapolation based on the measured AOT at 1020 nm and AE (870–1020 nm).

The way to obtain the column-integrated particle number concentrations APC_{50} and APC_{250} from the basic AERONET information (column-integrated particle volume size distribution) is described in detail in Mamouri and Ansmann (2015) (see Sect. 3.2 and

5

10

15

20

25

Lidar profiling of CCN- and INP-relevant aerosol parameters

R. E. Mamouri and
A. Ansmann

Title Page

Abstract

Introduction

Conclusions

References

Tables

Figures

◀

▶

◀

▶

Back

Close

Full Screen / Esc

Printer-friendly Version

Interactive Discussion



Fig. 3 in that article). The particle volume size distribution is retrieved for 22 logarithmically equidistant discrete radius points r_j with index j from 1 to 22 (Dubovik and King, 2000; Dubovik et al., 2006). The particle radius range from $r_1 = 0.05$ to $r_{22} = 15 \mu\text{m}$ is covered. Each radius r_j represents a radius interval of logarithmically equal width. To obtain the particle number concentration for each individual radius class, we divide the volume concentration of a given radius interval (or for the discrete radius point r_j) by the volume of a single particle with radius r_j and multiply this ratio with the spectral integral width of 0.2716. Unfortunately, we left out this multiplication with the dimensionless spectral width in the foregoing paper (Mamouri and Ansmann, 2015) so that the derived number concentrations APC_{280} (considering all particles with radius of about $> 280 \text{ nm}$, i.e., all particles in the radius classes 8–22) in Mamouri and Ansmann (2015) are a factor of $1/0.2716 (= 3.68)$ too high and also the respective APC_{280} -to-AEC conversion factor in Fig. 4 of that paper.

APC_{50} is the sum of the number concentrations of all classes from 1–22 and thus covers the full size range of optically active particles (at measured ambient humidity conditions). APC_{50} is our aerosol proxy in the estimation of APC_{CCN} (reservoir of potential CCN).

Regarding the large particles, we now switch from APC_{280} (Mamouri and Ansmann, 2015) to APC_{250} to be in full accordance with the INPC parameterization of DeMott et al. (2010, 2015). APC_{250} is about 10–20 % larger than APC_{280} which was used in Mamouri and Ansmann (2015) for simplicity. APC_{250} is the sum of the particle number concentrations of the radius classes 8–22 plus an additional contribution by radius class 7 (centered at $r_7 = 255 \text{ nm}$). This additional contribution is obtained by calculating the mean number concentration of the two intervals 7 and 8 (centered at $r_8 = 335 \text{ nm}$), assuming that this mean value represents the number concentration for the radius interval from 255 to 335 nm (centered at about 295 nm), and then taking 50 % of the computed mean value to consider only one half of the size interval. This latter value is interpreted as the number concentration of particles with radius from 250 to 295 nm.

Lidar profiling of CCN- and INP-relevant aerosol parameters

R. E. Mamouri and A. Ansmann

[Title Page](#)

[Abstract](#)

[Introduction](#)

[Conclusions](#)

[References](#)

[Tables](#)

[Figures](#)

[|◀](#)

[▶|](#)

[◀](#)

[▶](#)

[Back](#)

[Close](#)

[Full Screen / Esc](#)

[Printer-friendly Version](#)

[Interactive Discussion](#)



The total particle surface area concentration ASC is obtained by (a) computing the surface area of a sphere with radius r_j for all 22 classes, (b) multiplying the obtained surface areas for the particles with radius r_j with the number concentrations of radius interval j (obtained from the foregoing calculation of APC_{50} and APC_{250}), and (c) calculating the total surface area concentration by adding all contributions of the 22 size classes up. According to Weinzierl et al. (2009), ASC after AERONET is almost 98 % of the total ASC for coarse-mode dominating size distributions (i.e., in the case of mineral dust and marine aerosol). By inspection of all in-situ-measured size distribution at Leipzig within 2008 we found that ASC after AERONET is almost 0.95 of the total ASC. As reported by Granados-Muñoz et al. (2015), the size distribution retrieval uncertainties are 10–35 % for the particle radius range from 100 nm to 7 μm , and 80–100 % outside this range. The uncertainties in the integral values APC_{50} , APC_{250} , and ASC is estimated to be of the order of 10–20 % (Mamouri and Ansmann, 2015).

2.2 Aerosol lidars

The AERONET station of CUT at Limassol is equipped with a polarization/Raman lidar and belongs to the European Aerosol Research Lidar Network EARLINET (Pappalardo et al., 2014). The CUT lidar is described by Mamouri et al. (2013) and Nisantzi et al. (2015). In Sect. 5, we also show a lidar measurement obtained with a mobile system of the Polly^{XT} (POrtabLe Lidar sYstem, XT: extended version) series (Engelmann et al., 2015; Baars et al., 2015). This new Polly^{XT} was built by TROPOS for the National Observatory Athens (NOA) in 2014. The multiwavelength Raman/polarization lidar was extensively tested and characterized at Nicosia, Cyprus, during a six-week field campaign in March–April 2015. The field campaign was performed in the framework of the BACCHUS (impact of Biogenic vs. Anthropogenic emissions on Clouds and Climate: towards a Holistic UnderStanding, www.bacchus-env.eu) project. BACCHUS is a European Union's Seventh Framework Programme for Research (FP7) collaborative project of 20 institutes (including CUT and TROPOS), coordinated by ETH Zurich, Switzerland. The BACCHUS Cyprus 2015 field campaign focussed on ground-based and airborne

[Title Page](#)[Abstract](#)[Introduction](#)[Conclusions](#)[References](#)[Tables](#)[Figures](#)[|◀](#)[▶|](#)[◀](#)[▶](#)[Back](#)[Close](#)[Full Screen / Esc](#)[Printer-friendly Version](#)[Interactive Discussion](#)

in-situ observations of INPC and comparison of these observations with lidar-derived INPC profiles.

The retrieval of the basic lidar products (height profiles of particle optical properties) is explained in the next section. In the analysis of lidar data, we need to compute and correct for the contributions of clear air backscattering and extinction (Rayleigh scattering) to the measured backscatter and extinction coefficients. Actual height profiles of temperature and pressure profiles were used in the calculation of the Rayleigh backscatter and extinction coefficients. We downloaded GDAS (Global Data Assimilation System) meteorological data of the National Weather Service's National Centers for Environmental Prediction (NCEP) for our computations. NOAA's Air Resources Laboratory (ARL, <https://www.ready.noaa.gov/gdas1.php>) NCEP model GDAS output archives contain these data. The temperature profiles are also used in the INPC parameterizations in Sect. 3.4.

3 Methodology

In this section, the equations for the conversion of the measured optical aerosol properties into the microphysical properties are presented. Figure 1 illustrates the general idea of our approach. All steps are explained in Sects. 3.1–3.4. Table 2 provides an overview of the different steps of the computations. Section 3.1 starts with a brief explanation how we derive and estimate the required height profiles of particle extinction coefficient (AEC) for the three aerosol components, i.e., for maritime aerosol (m), mineral dust (d), and continental pollution (c). In Sect. 3.2, we present the conversion methods to obtain the estimated height profiles of APC_{50} , APC_{250} , and ASC from the lidar-derived AEC profiles for the three aerosol types. In Sect. 3.3, we provide a parameterization which relates APC_{50} to the number concentration $\text{APC}_{\text{CCN},s}$ of potential CCN as a function of supersaturation s . In Sect. 3.4, we compile the available INPC parameterization schemes (DeMott et al., 2010, 2015; Niemand et al., 2012; Steinke et al., 2015) in which APC_{250} and ASC profiles are input data. Mamouri and Ansmann

Title Page	
Abstract	Introduction
Conclusions	References
Tables	Figures
◀	▶
◀	▶
Back	Close
Full Screen / Esc	
Printer-friendly Version	
Interactive Discussion	

(2015) already outlined the principle way to obtain INPC from APC₂₅₀ profiles for the mineral dust aerosol component.

3.1 Aerosol-type-dependent AEC profiles from lidar

The main steps of our calculations from the basic lidar-derived optical properties to the cloud-relevant aerosol parameters are given in Table 2. Figure 2 shows our exemplary lidar observation from the BACCHUS campaign. This case will be further used in Sect. 5 (lidar case study). In the first step, we determine height profiles of particle backscatter coefficient and particle linear depolarization ratio for the transmitted laser wavelength (Fig. 2, left panel). These profiles allow us to separate the dust backscatter coefficient from non-dust backscatter contributions (Fig. 2, center). This part of the data analysis is explained in detail by Tesche et al. (2009), Groß et al. (2011), Mamouri et al. (2013), Mamouri and Ansmann (2014), and Nisantzi et al. (2015), and will therefore not be outlined here. By means of backward trajectories used to identify aerosol source regions and AERONET observations of AE and fine-mode fraction of 500 nm AOT (at the lidar site) we estimate the potential contribution of marine particles to the measured non-dust backscatter coefficient. In general, we assume that marine particles only occur in the boundary layer, e.g., at Cyprus up to 500 m at Limassol and up to about 1000–1500 m at Nicosia, and that the maritime AOT is < 0.05. In the free troposphere, the non-dust backscatter coefficient is assumed to be exclusively caused by anthropogenic haze and biomass burning smoke (denoted as continental pollution). This aerosol type includes also the natural aerosol component of biogenic particles, although not a man-made aerosol.

After a careful backscatter separation we multiply the three backscatter profiles with respective lidar ratios (35–40 sr for Middle East dust, 45 and 55 sr for eastern and western Saharan dust, respectively, 35–75 sr for continental non-dust aerosol, and 15–20 sr for marine particles) to obtain the AEC profiles for the three aerosol components (see Figs. 1 and 2, right panel). The overall uncertainty in the AEC retrieval is estimated to be of the order of 15–25 % for the dust extinction profile and 20–40 % for the non-

Title Page

Abstract

Introduction

Conclusions

References

Tables

Figures

|◀

▶|

◀

▶

Back

Close

Full Screen / Esc

Printer-friendly Version

Interactive Discussion



dust backscatter components (Tesche et al., 2009; Mamouri et al., 2013; Mamouri and Ansmann, 2014). A significant source of uncertainty is the lidar ratio for continental pollution which can vary between about 35 sr for almost non-absorbing anthropogenic haze and 75 sr for strongly absorbing biomass burning smoke (Müller et al., 2007; Groß et al., 2013).

With the help of actual AE values from AERONET observations, backward trajectories and the Raman-lidar solutions for the total particle extinction profile (Mattis et al., 2004; Baars et al., 2012, 2015; Kanitz et al., 2014), which are available for the lowest 2 km at daytime and for the full troposphere during nighttime in case of the Polly^{XT} lidar) (Engelmann et al., 2015), we are able to create a consistent and accurate aerosol mixture scenario throughout the troposphere up to cirrus level. In case of Raman-lidar extinction profiles, the sum of the three AEC profiles (for dust, marine, and continental pollution particles) in Fig. 2 (right panel) must match the Raman-lidar profile for the total particle extinction coefficient. Strong deviations then usually indicate a wrong estimate of the lidar ratio for continental aerosol pollution, as our experience shows.

3.2 Profiles of APC₅₀, APC₂₅₀, and ASC from the lidar AEC profiles

Based on the AEC profiles for marine, continental pollution, and dust particles we can estimate the microphysical aerosol properties (see Fig. 1) in the next step. In accordance with Shinozuka et al. (2015), we use the following approach to estimate APC₅₀ from AEC for aerosol type i :

$$n_{P50,i}(z) = c_{P50,i} \times \sigma_i^{x_i}(z) \quad (1)$$

with $n_{P50,i}$ in cm^{-3} , the conversion factor $c_{P50,i}$ in cm^{-3} for the particle extinction coefficient $\sigma_i = 1 \text{ Mm}^{-1}$, the particle extinction coefficient σ_i in Mm^{-1} , and the aerosol extinction exponent x_i . Equation (1) assumes a linear correlation of logAPC₅₀ with logAEC. Values for $c_{P50,i}$ and x_i are given in Table 3 for the three defined aerosol types and for all three laser wavelengths. In the equations of this section, we leave out to introduce a laser wavelength index in order to keep the terms in the equations as simple

Title Page

Abstract

Introduction

Conclusions

References

Tables

Figures

|◀

▶|

◀

▶

Back

Close

Full Screen / Esc

Printer-friendly Version

Interactive Discussion

Lidar profiling of CCN- and INP-relevant aerosol parameters

R. E. Mamouri and
A. Ansmann

[Title Page](#)

[Abstract](#)

[Introduction](#)

[Conclusions](#)

[References](#)

[Tables](#)

[Figures](#)

[|◀](#)

[▶|](#)

[◀](#)

[▶](#)

[Back](#)

[Close](#)

[Full Screen / Esc](#)

[Printer-friendly Version](#)

[Interactive Discussion](#)



as possible. The way how we obtained the specific, aerosol-type-dependent values of the conversion parameters in Table 3 is explained in Sect. 4.

APC_{250} for aerosol type i is related to the corresponding particle extinction coefficient AEC as follows:

$$n_{\text{P}250,i}(z) = c_{\text{P}250,i} \times \sigma_i(z) \quad (2)$$

with $n_{\text{P}250,i}$ in cm^{-3} , the conversion factor $c_{\text{P}250,i}$ in $\text{cm}^{-3} \text{Mm}$, and the particle extinction coefficient σ_i in Mm^{-1} . Equation (2) assumes a linear relationship between the large particle fraction APC_{250} and AEC. Again, the conversion factors are listed in Table 3.

Finally, we obtain the particle surface area concentration ASC for aerosol type i from

$$s_{\text{P},i}(z) = c_{\text{PS},i} \times \sigma_i(z) \quad (3)$$

with $s_{\text{P},i}$ in $\text{m}^2 \text{cm}^{-3}$ and the conversion factor $c_{\text{PS},i}$ in $\text{m}^2 \text{cm}^{-3} \text{Mm}$. Again, a linear relationship between particle surface area ASC and particle extinction coefficient AEC is assumed. The $c_{\text{PS},i}$ values are listed in Table 3. The overall uncertainties in all retrievals will be discussed in Sects. 4 and 5. Standard deviations of all conversion parameters in Table 3 are the basic information in the uncertainty analysis.

3.3 Profiles of $\text{APC}_{\text{CCN},s,i}$ from APC_{50}

We introduce $\text{APC}_{\text{CCN},s,i}$ as the particle number concentration of aerosol type i , which represents the potential CCN reservoir for a given supersaturation s (with respect to relative humidity over liquid water). We estimate $\text{APC}_{\text{CCN},s,i}$ from APC_{50} by using the following simple relationships:

$$n_{\text{CCN},0.15\%,i}(z) = 1.0 \times n_{\text{P}50,i}(z), \quad (4)$$

$$n_{\text{CCN},0.25\%,i}(z) = 1.35 \times n_{\text{P}50,i}(z), \quad (5)$$

$$n_{\text{CCN},0.40\%,i}(z) = 1.7 \times n_{\text{P}50,i}(z). \quad (6)$$

According to the literature, aerosol particles with radius of about > 40 nm (at $s = 0.25\%$, APC_{40}) and > 30 nm (at $s = 0.4\%$, APC_{30}) form the reservoir of potential CCN (Quinn et al., 2008; Rose et al., 2010; Deng et al., 2011; Ditas et al., 2012; Siebert et al., 2013; Henning et al., 2014). This was found from a variety of studies conducted in very different regions of the world and for very different aerosol mixtures. Only for supersaturation values of 0.2 % and lower, APC_{50} seems to represent the particle number concentration of the CCN reservoir.

By inspection of the size distributions for pure marine aerosols (Bates et al., 2000), pure dust particles (Weinzierl et al., 2009), continental pollution aerosol (Beddows et al., 2014), and own Leipzig city size distributions (measured at TROPOS in 2008), we found $\text{APC}_{30}/\text{APC}_{50}$ ratios on the order of 1.7 (± 0.8) and $\text{APC}_{40}/\text{APC}_{50}$ of about 1.35 (± 0.7) and used these as the enhancement factors of 1.35 and 1.7 in the above equations. Ji and Shaw (1998) found for pure ammonium sulfate in laboratory studies enhancement factors of 1.26 ($s = 0.25\%$) and 1.46 ($s = 0.4\%$) instead of 1.35 and 1.7 in the equations above, respectively. Shinozuka et al. (2015) assumes an increase of APC_{CCN} by a factor of 2 when the supersaturation increases from 0.2 to 0.4 %. Hirano et al. (2011) however also mentioned that natural aerosols show a much more complex behavior regarding these enhancement factors than considered in the equations above. All these uncertainties lead to the conclusion of Shinozuka et al. (2015) that the uncertainty range for $\text{APC}_{\text{CCN},s,i}$ is best described by a factor of 2–3 around the derived solutions.

3.4 Profiles of INPC from APC_{250} and ASC profiles

The final step of the retrieval (see Table 2 and Fig. 1) consists of the estimation of INPC profiles from the retrieved APC_{250} and ASC profiles. Different parameterizations can be used based on APC_{250} (DeMott et al., 2010, 2015) or ASC profiles (Niemand et al., 2012; Steinke et al., 2015).

Lidar profiling of CCN- and INP-relevant aerosol parameters

R. E. Mamouri and
A. Ansmann

[Title Page](#)

[Abstract](#) [Introduction](#)

[Conclusions](#) [References](#)

[Tables](#) [Figures](#)

◀

▶

Back

Close

Full Screen / Esc

[Printer-friendly Version](#)

[Interactive Discussion](#)



3.4.1 Estimation of INPC from APC₂₅₀

The INPC parameterizations introduced by DeMott et al. (2010, 2015) hold for APC₂₅₀(p_0, T_0) and thus standard (std) pressure ($p_0 = 1013 \text{ hPa}$) and temperature ($T_0 = 273.16 \text{ K}$) conditions (see Eqs. 7 and 8). Therefore, we have to convert each profile value APC₂₅₀(p_z, T_z) from ambient pressure p_z and temperature T_z at height z to APC₂₅₀(p_0, T_0) by using the factor $(T_z p_0)/(T_0 p_z)$.

DeMott et al. (2010) introduced a so-called global (aerosol-type-independent) INPC parameterization. We use this for continental pollution:

$$n_{\text{INP},c}(p_0, T_0, T_z) = a_1(273.16 - T_z)^{b_1} \times n_{\text{P250},c}(p_0, T_0)^{[c_1(273.16 - T_z) + d_1]} \quad (7)$$

with $n_{\text{P250},c}$ in std cm⁻³ representing APC_{250,c} for continental pollution, n_{INP} in std L⁻¹ representing INPC, $a_1 = 0.0000594$, $b_1 = 3.33$, $c_1 = 0.0265$, $d_1 = 0.0033$, and temperature $T(z)$ in K (and < 273.16 K). Note that the values of a_1 , b_1 , c_1 and d_1 given in Mamouri and Ansmann (2015) are erroneous. However, all computations presented in that paper were performed with the correct values listed here.

The INPC parameterization scheme for mineral dust is (DeMott et al., 2015):

$$n_{\text{INP},d}(p_0, T_0, T_z) = f_d n_{\text{P250},d}(p_0, T_0)^{[a_2(273.16 - T_z) + b_2]} \times \exp[c_2(273.16 - T_z) + d_2] \quad (8)$$

with the so-called atmospheric correction factor $f_d = 3$, and the coefficients $a_2 = 0.0$, $b_2 = 1.25$, $c_2 = 0.46$, and $d_2 = -11.6$.

Finally, we transfer the obtained INPC values $n_{\text{INP},c}(p_0, T_0, T_z)$ and $n_{\text{INP},d}(p_0, T_0, T_z)$ to the ones for ambient pressure and temperature conditions, $n_{\text{INP},c}(p_z, T_z)$ and $n_{\text{INP},d}(p_z, T_z)$, by multiplying $n_{\text{INP},c}(p_0, T_0, T_z)$ and $n_{\text{INP},d}(p_0, T_0, T_z)$ with the factor $(T_0 p_z)/(T_z p_0)$.

According to DeMott et al. (2010, 2015), Eqs. (7) and (8) can be used to estimate INPC for immersion freezing processes. The formulas are applicable to the temperature range from -9 to -35 °C (Eq. 7) and -21 to -35 °C (Eq. 8). In the result section (Sect. 4), we use these immersion-freezing-based parameterizations for higher as well

Title Page

Abstract

Introduction

Conclusions

References

Tables

Figures

◀

▶

◀

▶

Back

Close

Full Screen / Esc

Printer-friendly Version

Interactive Discussion



Title Page

Abstract

Introduction

Conclusions

References

Tables

Figures

◀

▶

Back

Close

Full Screen / Esc

Printer-friendly Version

Interactive Discussion

as lower temperatures. According to Wex et al. (2014) ice nucleation for anthropogenic particles and coated mineral dust particles (coated with natural and/or anthropogenic soluble material) can be described as immersion freezing as well. Above the deliquescence relative humidity, additional water is added to the coating and a solution shell forms around the particles, causing them to nucleate ice from concentrated solutions via the immersion freezing pathway, taking a freezing point depression into account.

5

Regarding uncertainties in the INPC computation, we assume that Eq. (7) allows a prediction of INPC within an uncertainty range of a factor of 5–10. DeMott et al. (2010) pointed out that an INPC uncertainty of an order of magnitude is still acceptable for cloud process modeling. The uncertainties are lower and within a factor of 2 when 10 using Eq. (8) (DeMott et al., 2015) for mineral dust. We leave out to present an INPC parameterization (similar to the ones introduced above) for marine particles.

3.4.2 Estimation of INPC from ASC

15

INPC profiles can also be estimated from the ASC profiles. An immersion-freezing INPC parameterization is provided by Niemand et al. (2012):

$$n_{\text{INP,d}}(T_z) = 1000 \times s_{\text{P,d}}(z) \times \eta_{\text{im}}(T_z), \quad (9)$$

$$\eta_{\text{im}}(T_z) = \exp[-0.517(T_z - 273.16) + 8.934], \quad (10)$$

20

with $n_{\text{INP,d}}$ in L^{-1} , $s_{\text{P,d}}$ in $\text{m}^2 \text{cm}^{-3}$ (so that a multiplication by 1000 is needed to obtain ASC in $\text{m}^2 \text{L}^{-1}$), and η_{im} in m^{-2} . The INPC profile holds from 237–261 K (−12 to -37°C).

Steinke et al. (2015) provides a deposition-freezing parameterization:

$$n_{\text{INP,d}}(T_z) = 1000 \times s_{\text{P,d}}(z) \times \eta_{\text{dep}}(T_z), \quad (11)$$

$$\eta_{\text{dep}}(T_z) = 1.88 \times 10^5 \times \exp(0.2659\chi(T_z)), \quad (12)$$

$$\chi(T_z) = -(T_z - 273.16) + (S_{\text{ICE}} - 1) \times 100, \quad (13)$$

with ice supersaturation of S_{ICE} . We assume $S_{\text{ICE}} = 1.15$ in Sect. 5. The INPC profile holds for temperatures from 220–253 K (-20 to -53 °C). Deposition-freezing INPC for the non-dust aerosol components (predominantly continental pollution) may also be estimated with the parameterization scheme after Steinke et al. (2015).

4 AERONET observations of the relationships of APC and ASC with AEC

Of key importance for the entire retrieval of cloud-relevant microphysical aerosol parameters from lidar-derived particle extinction coefficient profiles is the availability of trustworthy conversion parameters $c_{\text{P}50,i}$, $c_{\text{P}250,i}$, and $c_{\text{PS},i}$ and the aerosol extinction exponent x_i , which are required to solve Eqs. (1)–(3). These conversion parameters are derived from the long-term AERONET observations at Leipzig, Limassol, and Ragged Point, and the short-term dust-related field campaigns in Morocco, Cabo Verde, and Barbados (see Table 1). The main results of the AERONET data analysis are presented and discussed in this section. We performed the analysis of the link between the optical and microphysical aerosol parameters separately for all three laser wavelengths, but exemplarily show the results for the mostly used lidar wavelength of 532 nm.

To facilitate the AERONET data analysis and to be in full consistency with the CCNC-vs-AEC study of Shinozuka et al. (2015), we replaced all column integrals, i.e., the column values of APC_{50} , APC_{250} , ASC, and AOT, by respective volume-related values. For this, we introduced a normalizing, arbitrarily selected vertical column height of 1000 m, and divided all basic AERONET observational data points by 1000 m. An example of the transformation is illustrated in Fig. 3 for the Leipzig observation of the column-integrated APC_{250} and AOT at 532 nm. The volume-related values can be interpreted as the vertical averages of APC, ASC, and AEC in the assumed 1000 m deep column. It should be mentioned that the selected column height has no impact on the data analysis, but is set to a realistic value so that the range of AEC, typically measured with lidar for a given site, is covered.

Title Page

Abstract

Introduction

Conclusions

References

Tables

Figures

|◀

▶|

◀

▶

Back

Close

Full Screen / Esc

Printer-friendly Version

Interactive Discussion

4.1 Leipzig and Limassol long-term observations of mixed aerosols

We begin the presentation and discussion with the results for the multi-year observations at Leipzig, Germany, and Limassol, Cyprus. We used level-1.5 (Leipzig) and level-2.0 (Limassol) data. The observed correlations of APC_{50} , APC_{250} , and ASC vs 532 nm 5 AEC for pollution-dominated scenarios (\AAngstr\"om exponents $\text{AE} > 1.4$ and > 1.6) and for dust-dominated cases ($\text{AE} < 0.7$ and < 0.5) are shown in Figs. 4 and 5. At both sites a large variability in aerosol conditions occurs throughout each year. Limassol in 10 the eastern Mediterranean experiences complex aerosol conditions almost every day. This Middle East (Eastern Mediterranean) station is influenced by frequent dust outbreaks from the Sahara and the Middle East deserts (Nisantzi et al., 2015), biomass burning smoke and fire-induced soil dust injections (Nisantzi et al., 2014) from Turkey, the Black Sea area, and European regions further to the north, and anthropogenic haze from eastern, southeastern and southern Europe, northern Africa, and western Asia. Marine particles form the background aerosol at Limassol at the south coast of 15 Cyprus. In contrast, the central European AERONET station of Leipzig is heavily influenced by fresh and aged anthropogenic pollution, which dominates the boundary layer aerosol (Wandinger et al., 2004). A few Saharan dust outbreaks towards central Europe (Ansmann et al., 2003; Papayannis et al., 2008) and long-range transport of biomass burning aerosol and anthropogenic haze from southern Europe and North 20 America determine the aerosol conditions in the free troposphere (Mattis et al., 2008). On average, the FT AOT contributes 20 % to the overall AOT (Mattis et al., 2004). The impact of marine aerosol on the Leipzig observations is negligible.

Although complex aerosol mixtures always occur over Leipzig and Limassol, a considerable number of dust-dominated observations ($\text{AE} < 0.5$, all solid red circles in 25 Figs. 4 and 5) could be taken over the years and a comparably large number of measurements during events with dominating anthropogenic haze and biomass burning conditions ($\text{AE} > 1.6$, all solid green circles in the figures) is available (see Table 1). We used AE calculated from the AOT values from 440 to 870 nm here to filter out

[Title Page](#)[Abstract](#)[Introduction](#)[Conclusions](#)[References](#)[Tables](#)[Figures](#)[|◀](#)[▶|](#)[Back](#)[Close](#)[Full Screen / Esc](#)[Printer-friendly Version](#)[Interactive Discussion](#)

dust-dominated and haze-dominated aerosol observations. The available numbers of AERONET observations for each of the two aerosol sub data sets are given in Table 1.

The found scatter in the correlations of APC_{50} , APC_{250} , and ASC with AEC is caused by many reasons. First of all, different particle size distributions (leading to different 5 APC and ASC values) can produce the same AEC value. The optical efficiency (optical cross section divided by the geometrical cross section ASC/4) of a given log-normal aerosol size distribution can easily vary between 0.3 and 3 as a function of a shifting mode radius of the fine-mode particle spectrum towards larger or smaller sizes without leading to significant changes in the APC and ASC values. The particle optical effects depend on ambient relative humidity (significant water up-take by particles when 10 the relative humidity in the vertical column exceeds 70 %) so that large changes in AEC (within a factor of 1.5–2.5) may be correlated with only small changes in APC_{50} , APC_{250} , and ASC. The aerosol mixtures (or the overall chemical composition of the particles including the type-dependent water uptake and growth effects) may be different 15 for relatively clean aerosol conditions (low AEC values) and scenarios with heavy pollution or dust outbreaks (high AEC values). This may systematically influence the correlation features.

In consistency with the study of the CCN–AEC relationship by Shinozuka et al. (2015), we applied the regression analysis to the $\log\text{APC}_{50}$ – $\log\text{AEC}$ data field for each 20 of the two data sets (top panels in Figs. 4 and 5). The regression lines in the figures go through the geometric averages of APC_{50} and AEC. The slope of the regression line is the extinction exponent x in Eq. (1). As Shinozuka et al. (2015) pointed out, the $10^{\text{intercept}}$ (which is $c_{\text{P}50,i}$ in Eq. 1) of the linear fit made on the \log_{10} – \log_{10} coordinates is an estimate of the geometric mean of APC_{50} at AEC of 1 Mm^{-1} . The obtained 25 numbers for x and $c_{\text{P}50,i}$ (for 532 nm) are given in Table 3 (Cyprus and Germany observations). The standard deviation (root mean square values are mostly 0.2–0.3 in the log scale) of the regressions analysis indicates uncertainties within a factor of 1.5–2 in the retrieval of APC_{50} from AEC.

Title Page

Abstract

Introduction

Conclusions

References

Tables

Figures

|◀

▶|

◀

▶|

Back

Close

Full Screen / Esc

Printer-friendly Version

Interactive Discussion

The results are in good agreement with the study of measured CCN–AEC relationships by Shinozuka et al. (2015). They used the 500 nm AEC for dried particles instead of AEC for ambient humidity conditions as used in our study. Similar slopes from 0.76 ± 0.10 to 0.87 ± 0.06 were reported for different continental sites in North America and Europe for anthropogenic pollution (for AE from 1.5–1.7). For dust-dominated aerosols (AE from 0.3–0.5) they obtained slopes from 0.45 ± 0.04 to 0.90 ± 0.06 . For a German site (Black Forest) the slope is 0.87 ± 0.06 and the ratio of CCNC for $s = 0.4\%$ to dry-particle AEC^{0.87} is 27.8. This ratio is similar to our value of 35.0 for the ratio of APC₅₀ to ambient AEC^{0.90}.

Liu and Li (2014) showed that the product of AEC × AE (denoted as Aerosol Index AI, introduced by Nakajima et al., 2001) provides a better correlation with CCNC (or APC₅₀) than CCNC with AEC. By using AI instead of AEC in the correlation, Liu and Li (2014) indirectly consider information on the aerosol type (high AI for fine-mode-dominated aerosol, low AI for coarse-mode-dominated aerosol conditions). Similarly, Shinozuka et al. (2015) separated the observations in classes with AE from 1.5–1.7 and from 0.3–0.5. In their study, $c_{P50,i}$ in Eq. (1) is also a function of AE so that different aerosol types can be handled with one type of parameterization. In contrast, we separate the different aerosol types by means of the polarization lidar technique before we apply our parameterization and conversion procedures to estimate the microphysical and cloud-relevant aerosol parameters.

A complex regression data analysis as in the top panels of Figs. 4 and 5 is not needed in the study of the APC₂₅₀–AEC and ASC–AEC relationships. We can assume simple linear relationships because the optical effects of the aerosol mixtures depend approximately linearly on ASC and APC₂₅₀. For all individual, single AERONET observations (belonging to the separate data sets with AE > 1.6 and AE < 0.5) we calculated the APC₂₅₀/AEC and ASC/AEC ratios for all three laser wavelengths. In Figs. 4 and 5, the geometrical averages of these ratios (for 532 nm AEC) define the slopes of the shown straight lines. Shown are both slopes for the fine-mode and coarse mode classes. The mean values of APC₂₅₀/AEC and ASC/AEC for each aerosol subdata set (AE < 0.5,

Lidar profiling of CCN- and INP-relevant aerosol parameters

R. E. Mamouri and
A. Ansmann

[Title Page](#)

[Abstract](#)

[Introduction](#)

[Conclusions](#)

[References](#)

[Tables](#)

[Figures](#)

[|◀](#)

[▶|](#)

[Back](#)

[Close](#)

[Full Screen / Esc](#)

[Printer-friendly Version](#)

[Interactive Discussion](#)



$\text{AE} > 1.6$) are used as $c_{\text{P}250,i}$ and $c_{\text{PS},i}$, respectively, in Eqs. (2) and (3). All Leipzig and Limassol values of $c_{\text{P}250,i}$ and $c_{\text{PS},i}$ and standard deviations (obtained from the averaging computation) for 355, 532, and 1064 nm are given in Table 3.

Our results are in good agreement with respective model studies for various aerosol types conducted by Barnaba and Gobbi (2001, 2002). According to Barnaba and Gobbi (2001), the ASC–AEC ratio for 500–550 nm should be in the range of 2–4 for particle size distributions with strong coarse mode (marine and dust particles causing a low AE). Kolgotin et al. (2015) found a value of 1.6 ($\pm 20\%$) for the ASC/AEC ratio at the 355 nm wavelength. In their simulations, they considered mono-modal log-normal size distributions with mean radius from 20 to 300 nm. We conclude from their study that the ASC/AEC values are in the range from 2.4–3 for 532 nm.

The deviation from the linear APC_{250} –AEC relationship for Leipzig with increasing AEC (for the $\text{AE} > 1.6$ data set) may indicate a change in the aerosol mixture (more dust particles) and/or also a stronger humidity effect (particle growth by water uptake with increasing AEC).

The scatter of the individual observations for the typical range of AEC from 50–400 Mm^{-1} provides insight into the uncertainty of the retrieval of the particle number concentrations and surface area concentrations for the measured particle extinction coefficients. The respective standard deviations of $c_{\text{P}250,i}$ and $c_{\text{PS},i}$ in Table 3 are used in the error analysis, which will be discussed in Sects. 4 and 5. The standard deviation roughly indicate that conversions of AEC into APC_{250} and ASC is possible with a relative error of 20–30 %. From the Leipzig and Limassol AERONET data analysis and the relative amount of data we may conclude that the Cyprus results (for $\text{AE} < 0.5$) are representative for mineral dust scenarios, whereas the Leipzig data (for $\text{AE} > 1.6$) may better describe continental aerosol pollution characteristics.

4.2 Field campaign data sets for pure dust conditions

Unique AERONET data sets are available for pure Saharan dust conditions, sampled during several field campaigns in southeastern Morocco, close to the dust source at

Lidar profiling of CCN- and INP-relevant aerosol parameters

R. E. Mamouri and
A. Ansmann

[Title Page](#)

[Abstract](#)

[Introduction](#)

[Conclusions](#)

[References](#)

[Tables](#)

[Figures](#)

[I◀](#)

[▶](#)

[◀](#)

[▶](#)

[Back](#)

[Close](#)

[Full Screen / Esc](#)

[Printer-friendly Version](#)

[Interactive Discussion](#)



a minimum influence by marine particles and anthropogenic pollution, at Cape Verde during a rather heavy dust outbreak from 28–30 January 2008, and at Barbados (lofted pure dust plumes during the summer months) in the long-range dust transport regime, 5000–8000 km west of the Saharan dust sources (see Table 1). We used level-1.5 AERONET data in the case of the Barbados observations and checked all measurements carefully regarding cloud contamination (subvisible and thin cirrus) by means of the accompanying SALTRACE lidar observations. When using level-2.0 data, many dust observations are removed, probably as a result of cloud screening. In the case of the Morocco and Cabo Verde, level-2.0 data are taken. Unfortunately, problems with the AERONET 340 nm channel in Morocco and Barbados prohibit the retrieval of conversion parameters at 355 nm. So, we present the conversion parameters at 380 nm in Table 3 which fairly well represent the parameters for 355 nm in the case mineral dust.

Because lidar observations of the vertical structures of the dust layers and thus information of the dust layer depth is available for all field campaigns, we can present correlations between layer mean APC and ASC and layer mean AEC, based on the individual lidar/photometer observations. The radiosonde profiles of relative humidity always indicated dry conditions in the dust layers (relative humidity < 50 %) so that water particle uptake and growth effects did not play a role in the correlation study.

The main results are shown in Fig. 6 (for 532 nm). The findings are given in the same way as for the multi-year Leipzig and Limassol data in Figs. 4 and 5. The relationship between the dust APC_{250} and AEC values was already discussed by Mamouri and Ansmann (2015). However, as mentioned in Sect. 2.1, a wrong conversion factor of 0.63 Mm cm^{-3} was used in the foregoing article, the true one is $c_{P250,d} = 0.19 \text{ Mm cm}^{-3}$. Figure 6 is now extended to cover the conversion parameters for dust APC_{50} and ASC. All obtained pure dust $c_{P50,i}$, X_i , $c_{P250,i}$ and $c_{PS,i}$ values and corresponding standard deviations for 355, 532, and 1064 nm are given in Table 3.

Lidar profiling of CCN- and INP-relevant aerosol parameters

R. E. Mamouri and
A. Ansmann

[Title Page](#)

[Abstract](#)

[Introduction](#)

[Conclusions](#)

[References](#)

[Tables](#)

[Figures](#)

[|◀](#)

[▶|](#)

[◀](#)

[▶](#)

[Back](#)

[Close](#)

[Full Screen / Esc](#)

[Printer-friendly Version](#)

[Interactive Discussion](#)



4.3 Pure marine aerosol conditions

Barbados offers also the unique opportunity to analyse the relationship between the microphysical and optical properties for pure marine conditions (during dust-free conditions). As mentioned, Barbados is located more than 4000 km west of Africa. No anthropogenic aerosol sources exists upwind Barbados over the tropical Atlantic (except ships). We used the 2007–2015 level 2.0 Ragged Point data set (see Table 1) and selected all observations with $500\text{ nm AOT} < 0.07$ and AE (440–870 nm) between 0.25 and 0.6 for our correlation study. Most AE values for marine conditions accumulate around 0.4–0.5 and are thus clearly larger than desert-dust-dominated AE values which accumulate around 0.1–0.2. At pure marine conditions, the relative humidity in the marine boundary layer is always above 75 % so that humidity and particle growth effects did not disturbed our marine aerosol study. The conversion parameters for pristine marine conditions are given in Table 3.

4.4 Summarizing overview

Figure 7 provides an overview of all 532 nm mean conversion parameters for the three aerosol types and different AERONET data sets. As can be seen, the Limassol conversion parameters for dust-dominated cases ($\text{AE} < 0.5$) are close the ones from the dust field campaigns. The error bars of the Leipzig dust parameters are considerably larger because of the impact of other aerosol types than dust during observations with $\text{AE} < 0.5$. Pure dust events are hard to measure over central Europe.

Marine parameters are close the ones for dust. This is caused by the fact that similar particle size distributions features (weak fine mode, pronounced coarse mode) are given for both, dust and marine particle ensembles.

There is no clear picture for anthropogenic pollution. Anthropogenic aerosols (mixed with smoke, fine-mode soil dust, and biogenic particles) over the Middle East station are obviously different from the ones over central Europe. Different absorption contribution to the particle extinction coefficient can partly explain the found differences

Discussion Paper	Discussion Paper	Title Page
		Abstract
		Introduction
		Conclusions
		References
		Tables
		Figures
	◀	▶
	◀	▶
	Back	Close
	Full Screen / Esc	
	Printer-friendly Version	
	Interactive Discussion	

in the conversion parameters. We use the Leipzig values in Sect. 5 (lidar application), because more AERONET data were available for Leipzig (see Table 1), and the Leipzig parameters are more close to the values obtained by Shinozuka et al. (2015) for polluted North American and European stations. Furthermore, the rather complex aerosol conditions over Cyprus may not allow to observe almost pure continental pollution cases at any time.

Regarding the uncertainties in the conversions we can conclude from our correlation studies that the overall uncertainties are described by a factor of 2 for APC_{50} , and that the uncertainties are on the order of 20–30 % in the conversion of AEC to APC_{250} and ASC. The uncertainties are similar for all three wavelengths.

5 Lidar estimates of $\text{APC}_{\text{CCN},s}$ and INPC profiles: case studies

In this section we apply the developed methodology presented in Sect. 3 to two lidar observations. The first lidar measurement was performed recently during a strong dust outbreak crossing Cyprus in the spring of 2015. The second case was measured during an episode with continental aerosol pollution advected from the European continent to Cyprus in the summer of 2012.

5.1 Lidar profiling during a dust outbreak

During the BACCHUS field campaign in March–April 2015, described in Sect. 2.2, many dust outbreaks from the Middle East deserts and the Sahara were observed over Cyprus. We selected the case from 7 April to apply our methods to a dust-dominated aerosol scenario. The basic lidar observations of height profiles of particle backscatter, linear depolarization ratio, and derived AEC profiles were already shown in Fig. 2. These 532 nm AEC profiles are the input parameters for the retrieval of the particle number concentrations APC_{50} and APC_{250} and of the particle surface area concentration ASC shown in Fig. 8. Equations (1)–(3) and the conversion parameters in Table 3

Lidar profiling of CCN- and INP-relevant aerosol parameters

R. E. Mamouri and
A. Ansmann

[Title Page](#)

[Abstract](#)

[Introduction](#)

[Conclusions](#)

[References](#)

[Tables](#)

[Figures](#)

[|◀](#)

[▶|](#)

[◀](#)

[▶](#)

[Back](#)

[Close](#)

[Full Screen / Esc](#)

[Printer-friendly Version](#)

[Interactive Discussion](#)



are used to obtain the shown profiles. For dust we used the SAMUM/SALTRACE conversion parameters, for continental pollution the Leipzig data (in the APC_{50} retrieval), the Leipzig and Limassol mean conversion factors in the calculation of APC_{250} and ASC profiles, and for marine aerosols the Barbados (2007–2015) conversion parameters.

We also show the respective profiles obtained from the 355 nm AEC profiles (Fig. 8, bottom) to demonstrate that ESA's EarthCARE lidar (satellite-borne 355 nm polarization/HSR lidar) (Illingworth et al., 2015) will allow us to retrieve these profiles on a global scale. Despite some differences in the extinction profiles for the different wavelengths, the profiles of the microphysical parameters are very similar.

The error bars indicate typical uncertainties caused by the uncertainties in the basic retrieval of the optical properties (Mamouri and Ansmann, 2015) and uncertainties in the conversion parameters. For APC_{50} we simply assume an overall uncertainty factor of 2. For APC_{250} and ASC, the error analysis revealed overall uncertainties of about 25–50 % for the dust-related profiles and 30–60 % for the APC_{250} and ASC profiles for continental aerosol pollution. The error bars in Fig. 8 indicate typical errors of 30 % (dust-related profiles) and 40 % (non-dust-related profiles).

Figure 9 (left panel) shows the retrieved profiles of $\text{APC}_{\text{CCN},s} = 0.15\%$ and $\text{APC}_{\text{CCN},s} = 0.4\%$. The profiles are computed with Eqs. (4) and (6). The derived INPC profiles (right panels) are computed with the available parameterization schemes after DeMott et al. (2010) (Eq. 7 with $\text{APC}_{250,c}(z)$ as input), DeMott et al. (2015) (Eq. 8 with $\text{APC}_{250,d}(z)$ as input), Niemand et al. (2012) (Eq. 10 with $\text{ASC}_d(z)$ as input, immersion freezing mode), and Steinke et al. (2015) (Eq. 13 with $\text{ASC}_d(z)$ as input, deposition freezing mode). The error bars for $\text{APC}_{\text{CCN},s} = 0.4\%$ show again the factor 2 uncertainty. For INPC, the uncertainty is characterized by a factor of 2–5.

Mamouri and Ansmann (2015) already discussed the retrieval of INPC from $\text{APC}_{250,d}$ (Fig. 9, D10 and D15 profiles). Figure 9 also contains the INPC profiles when ASC_d is used as input (N12, S15). Because air temperatures are all above 0 °C at heights below 3.6 km, INPC profiles only cover the upper part of the dust plume.

Lidar profiling of CCN- and INP-relevant aerosol parameters

R. E. Mamouri and
A. Ansmann

[Title Page](#)

[Abstract](#) [Introduction](#)

[Conclusions](#) [References](#)

[Tables](#) [Figures](#)

◀

▶

◀

▶

[Back](#)

[Close](#)

[Full Screen / Esc](#)

[Printer-friendly Version](#)

[Interactive Discussion](#)

[Title Page](#)

[Abstract](#)

[Introduction](#)

[Conclusions](#)

[References](#)

[Tables](#)

[Figures](#)

[|◀](#)

[▶|](#)

[◀](#)

[▶](#)

[Back](#)

[Close](#)

[Full Screen / Esc](#)

[Printer-friendly Version](#)

[Interactive Discussion](#)

To better highlight the differences between the different INP parameterization schemes, we shifted the temperature profile by 15 K towards lower temperatures. The resulting INPC profiles are shown in Fig. 10. The thick solid line segments show the temperature ranges for which the parameterizations are developed.

It is not the aim of the paper to discuss the quality of the different parameterizations and the reasons for the differences between the immersion freezing parameterizations after DeMott et al. (2015) and Niemand et al. (2012), which partly exceed one order of magnitude. However, the following general statements can be made: The INCP parameterization presented by DeMott et al. (2010) (here applied to the continental aerosol pollution) and by DeMott et al. (2015) (for mineral dust) enable us to calculate non-dust and dust INPC profiles for the temperature range in which immersion freezing is the dominating freezing mode. The higher dust INPC values obtained with the procedure developed by Niemand et al. (2012) compared to the one presented by DeMott et al. (2015) may result from the fact that ASC covers all particles even particles with radius < 250 nm. The combination of the parameterizations of Niemand et al. (2012) (dust aerosol, immersion freezing) and Steinke et al. (2015) (dust, deposition freezing) provides the opportunity to deliver INPC profiles from about -10 to -50 °C and thus up to cirrus level.

5.2 Lidar profiling during an episode with European continental pollution

In contrast to the BACCHUS dust case in Fig. 2, the backscatter and depolarization profiles in Fig. 11 show very different features during a period with strong advection of European continental pollution. The measurement was taken at Limassol on 16 August 2012. On that day, AE was close to 1.8 and the particle linear depolarization ratio below 10 %. Aerosols up to 4 km height were detected and the air masses came from northern to northwestern directions, from Europe and Turkey according to backward trajectory analysis. We used lidar ratios of 50–60 sr for continental pollution and 45 sr for mineral dust in the backscatter-to-extinction conversion, applied to obtain the AEC profiles.

In Fig. 11, we assume again a small contribution of marine particles in the marine boundary layer. The almost height-independent depolarization ratio indicates an aged well-mixed pollution plume with a minor contribution of dust (soil dust, road dust etc.). Figure 12 shows the derived profiles of the microphysical parameters APC_{50} , APC_{250} , and ASC. The respective APC_{CCN} profiles (not shown) are obtained by multiplying the APC_{50} profile by 1.35 ($s = 0.25\%$) and 1.7 ($s = 0.4\%$). INPC values are at all zero for this case with temperatures at all above 0 °C up to 5 km height.

The comparison of Fig. 8 (coarse-mode-dominated case) with Fig. 12 (fine-mode-dominated aerosol scene) reveals that the APC_{50} values are roughly a factor of 2 higher in the case with dominating continental pollution for similar values of the total (dust plus non-dust) 532 nm AEC. Similarly, the (total) ASC values are much higher in Fig. 12. This reflects that fine-mode-dominated particles ensembles show much higher Aitken and accumulation-mode particle number and surface area concentrations (for given fixed volume concentration) than coarse-mode-dominated aerosols.

At the end of our studies, the role of water uptake by particles on the retrieval of APC_{CCN} and INPC remains to be discussed. Especially for aerosol pollution scenarios, care has to be taken in the estimations of cloud-relevant particle properties because of potential water uptake effects close to cloud base. Schmidt et al. (2014) found that particle water uptake effects may be small at distances > 300 m below cloud base. In that study, the derived AEC profiles for about 30 altocumulus cloud cases showed a strong increase of the extinction coefficient within the 300 m layer below cloud base only. If relative humidity profiles are available (from nearby radiosonde ascents or Raman lidar profiling of the water-vapor mixing ratio in combination with the used model GDAS temperature profiles), the APC_{CCN} estimates should be interpreted with caution if the relative humidity exceeds 80–90 %.

Lidar profiling of CCN- and INP-relevant aerosol parameters

R. E. Mamouri and
A. Ansmann

[Title Page](#)

[Abstract](#)

[Introduction](#)

[Conclusions](#)

[References](#)

[Tables](#)

[Figures](#)

◀

▶

[Back](#)

[Close](#)

[Full Screen / Esc](#)

[Printer-friendly Version](#)

[Interactive Discussion](#)



6 Conclusions

Active remote sensing is needed for vertically resolved cloud process and aerosol-cloud-interaction studies. In this context it is of importance to investigate to what extend lidar, as the most prominent aerosol profiling technique, can provide cloud-relevant

- 5 aerosol properties. For the first time, we presented a comprehensive study which covers the relationship between lidar-derived aerosol optical properties and aerosol particle number concentrations relevant for liquid-water droplet nucleation and heterogeneous ice nucleation. We based our study on observations (AERONET) rather than model computations to obtain a realistic view on the potential and limits of the retrieval
10 technique presented here.

Of key importance is the polarization lidar which allows us to separate basic aerosol types such as mineral dust and continental pollution (smoke, haze) which have different cloud-influencing properties. We showed that height profiles of number concentrations of aerosol particles with radius $> 50 \text{ nm}$ (APC_{50} , reservoir of favorable CCN, denoted
15 as APC_{CCN}) and with radius $> 250 \text{ nm}$ (APC_{250} , reservoir of favorable INP), as well as profiles of the aerosol particle surface area concentration (ASC, used in INP parameterization) can be retrieved from lidar-derived aerosol extinction coefficients with relative uncertainties of a factor of around 2 (APC_{50}), and about 25–50 % (APC_{250} , ASC). We presented the necessary conversion parameters (for the conversion of optical into microphysical aerosol properties) for the main lidar wavelengths of 355, 532
20 and 1064 nm and main aerosol types (dust, pollution, marine particles).

The full methodology was applied to observations of a heavy dust outbreak crossing Cyprus with dust up to 8 km height in the spring of 2015 and to a case during which anthropogenic pollution dominated. For these cases the final products of the retrievals
25 (APC_{CCN} and INPC profiles) were shown and the retrieval uncertainties discussed.

Our future plans comprise extended comparisons of the lidar observations with respective surface and airborne in situ observations of aerosol microphysical properties and measured CCNC and INPC time series and profiles. These comparisons may allow

Title Page

Abstract

Introduction

Conclusions

References

Tables

Figures

◀

▶

Back

Close

Full Screen / Esc

Printer-friendly Version

Interactive Discussion

Title Page

Abstract

Introduction

Conclusions

References

Tables

Figures

◀

▶

Back

Close

Full Screen / Esc

Printer-friendly Version

Interactive Discussion



References

- Andreae, M. O.: Correlation between cloud condensation nuclei concentration and aerosol optical thickness in remote and polluted regions, *Atmos. Chem. Phys.*, 9, 543–556, doi:10.5194/acp-9-543-2009, 2009. 34152
- Ansmann, A., Bösenberg, J., Chaikovsky, A., Comerón, A., Eckhardt, S., Eixmann, R., Freudenthaler, V., Ginoux, P., Komguem, L., Linné, H., López Márquez, M. A., Matthias, V., Mattis, I., Mitev, V., Müller, D., Music, S., Nickovic, S., Pelon, J., Sauvage, L., Sobolewsky, P., Srivastava, M. K., Stohl, A., Torres, O., Vaughan, G., Wandinger, U., and Wiegner, M.: Long-range transport of Saharan dust to northern Europe: the 11–16 October 2001 outbreak observed with EARLINET, *J. Geophys. Res.*, 108, 4783, doi:10.1029/2003JD003757, 2003. 34167
- Ansmann, A., Wandinger, U., Le Rille, O., Lajas, D., and Straume, A. G.: Particle backscatter and extinction profiling with the spaceborne high-spectral-resolution Doppler lidar ALADIN: methodology and simulations, *Appl. Optics*, 46, 6606–6626, 2007. 34153
- Ansmann, A., Tesche, M., Seifert, P., Althausen, D., Engelmann, R., Fruntke, J., Wandinger, U., Mattis, I., and Müller, D.: Evolution of the ice phase in tropical altocumulus: SAMUM lidar observations over Cape Verde, *J. Geophys. Res.*, 114, D17208, doi:10.1029/2008JD011659, 2009. 34151, 34152
- Ansmann, A., Petzold, A., Kandler, K., Tegen, I., Wendisch, M., Müller, D., Weinzierl, B., Müller, T., and Heintzenberg, J.: Saharan mineral dust experiments SAMUM-1 and SAMUM-2: what have we learned?, *Tellus B*, 63, 403–429, doi:10.1111/j.1600-0889.2011.00555.x, 2011a. 34155
- Ansmann, A., Tesche, M., Seifert, P., Groß, S., Freudenthaler, V., Apituley, A., Wilson, K. M., Serikov, I., Linné, H., Heinold, B., Hiebsch, A., Schnell, F., Schmidt, J., Mattis, I., Wandinger, U., and Wiegner, M.: Ash and fine-mode particle mass profiles from EARLINET-AERONET observations over central Europe after the eruptions of the Eyjafjallajökull volcano in 2010, *J. Geophys. Res.*, 116, D00U02, doi:10.1029/2010JD015567, 2011b. 34153
- Ansmann, A., Seifert, P., Tesche, M., and Wandinger, U.: Profiling of fine and coarse particle mass: case studies of Saharan dust and Eyjafjallajökull/Grimsvötn volcanic plumes, *Atmos. Chem. Phys.*, 12, 9399–9415, doi:10.5194/acp-12-9399-2012, 2012. 34153
- Ansmann, A., Althausen, D., Kanitz, T., Engelmann, R., Skupin, A., Baars, H., Klepel, A., Haarig, M., Heinold, B., Tegen, I., Toledano, C., Prescod, D., and Farrell, D.: Saharan dust long-range transport: SALTRACE lidar observations at Barbados and aboard RV Meteor

ACPD

15, 34149–34204, 2015

Lidar profiling of CCN- and INP-relevant aerosol parameters

R. E. Mamouri and
A. Ansmann

Title Page

Abstract

Introduction

Conclusions

References

Tables

Figures

◀

▶

Back

Close

Full Screen / Esc

Printer-friendly Version

Interactive Discussion



5 Augustin, S., Wex, H., Niedermeier, D., Pummer, B., Grothe, H., Hartmann, S., Tomsche, L., Clauss, T., Voigtlander, J., Ignatius, K., and Stratmann, F.: Immersion freezing of birch pollen washing water, *Atmos. Chem. Phys.*, 13, 10989–11003, doi:10.5194/acp-13-10989-2013, 2013. 34152

10 Augustin-Bauditz, S., Wex, H., Kanter, S., Ebert, M., Stolz, F., Prager, A., Niedermeier, D., and Stratmann, F.: The immersion mode ice nucleation behavior of mineral dusts: a comparison of different pure and surface modified dusts, *Geophys. Res. Lett.*, 41, 7375–7382, doi:10.1002/2014GL061317, 2014. 34152

15 Baars, H., Ansmann, A., Althausen, D., Engelmann, R., Heese, B., Müller, D., Artaxo, P., Paixao, M., Pauliquevis, T., and Souza, R.: Aerosol profiling with lidar in the Amazon Basin during the wet and dry season, *J. Geophys. Res.*, 117, D21201, doi:10.1029/2012JD018338, 2012. 34161

20 Baars, H., Kanitz, T., Engelmann, R., Althausen, D., Heese, B., Komppula, M., Preißler, J., Tesche, M., Ansmann, A., Wandinger, U., Lim, J.-H., Ahn, J. Y., Stachlewska, I. S., Amiridis, V., Marinou, E., Seifert, P., Hofer, J., Skupin, A., Schneider, F., Bohlmann, S., Foth, A., Bley, S., Pfüller, A., Giannakaki, E., Lihavainen, H., Viisanen, Y., Hooda, R. K., Pereira, S., Bortoli, D., Wagner, F., Mattis, I., Janicka, L., Markowicz, K. M., Achtert, P., Artaxo, P., Pauliquevis, T., Souza, R. A. F., Sharma, V. P., van Zyl, P. G., Beukes, J. P., Sun, J. Y., Rohwer, E. G., Deng, R., Mamouri, R. E., and Zamorano, F.: Polly^{NET}: a global network of automated Raman-polarization lidars for continuous aerosol profiling, *Atmos. Chem. Phys. Discuss.*, 15, 27943–28004, doi:10.5194/acpd-15-27943-2015, 2015. 34158, 34161

25 Barnaba, F. and Gobbi, G. P.: Lidar estimation of tropospheric aerosol extinction, surface area and volume: maritime and desert-dust cases, *J. Geophys. Res.*, 106, 3005–3018, doi:10.1029/2000JD900492, 2001. 34154, 34170

30 Barnaba, F. and Gobbi, G. P.: Correction to “Lidar estimation of tropospheric aerosol extinction, surface area and volume: maritime and desert-dust cases” by F. Barnaba and G. P. Gobbi, *J. Geophys. Res.*, 107, 4180, doi:10.1029/2002JD002340, 2002. 34170

Bates, T. S., Quinn, P. K., Covert, D. S., Coffman, D. J., Johnson, J. E., and Wiedensohler, A.: Aerosol physical properties and processes in the lower marine boundary layer: a com-

Lidar profiling of CCN- and INP-relevant aerosol parameters

R. E. Mamouri and
A. Ansmann

Title Page

Abstract

Introduction

Conclusions

References

Tables

Figures

◀

▶

Back

Close

Full Screen / Esc

Printer-friendly Version

Interactive Discussion



Lidar profiling of CCN- and INP-relevant aerosol parameters

R. E. Mamouri and
A. Ansmann

[Title Page](#)

[Abstract](#)

[Introduction](#)

[Conclusions](#)

[References](#)

[Tables](#)

[Figures](#)

[|◀](#)

[▶|](#)

[◀](#)

[▶](#)

[Back](#)

[Close](#)

[Full Screen / Esc](#)

[Printer-friendly Version](#)

[Interactive Discussion](#)



parison of shipboard sub-micron data from ACE-1 and ACE-2, Tellus B, 52, 258–272, doi:10.1034/j.1600-0889.2000.00021.x, 2000. 34163

5 Beddows, D. C. S., Dall'Osto, M., Harrison, R. M., Kulmala, M., Asmi, A., Wiedensohler, A., Laj, P., Fjaeraa, A. M., Sellegrí, K., Birmili, W., Bukowiecki, N., Weingartner, E., Baltensperger, U., Zdimal, V., Zikova, N., Putaud, J.-P., Marinoni, A., Tunved, P., Hansson, H.-C., Fiebig, M., Kivekäs, N., Swietlicki, E., Lihavainen, H., Asmi, E., Ulevicius, V., Aalto, P. P., Mihalopoulos, N., Kalivitis, N., Kalapov, I., Kiss, G., de Leeuw, G., Henzing, B., O'Dowd, C., Jennings, S. G., Flentje, H., Meinhardt, F., Ries, L., Denier van der Gon, H. A. C., and Visschedijk, A. J. H.: Variations in tropospheric submicron particle size distributions across the European continent 2008–2009, Atmos. Chem. Phys., 14, 4327–4348, doi:10.5194/acp-14-4327-2014, 2014. 34163

Bühl, J., Ansmann, A., Seifert, P., Baars, H., and Engelmann, R.: Toward a quantitative characterization of heterogeneous ice formation with lidar/radar: comparison of CALIPSO/CloudSat with ground-based observations, Geophys. Res. Lett., 40, 4404–4408, doi:10.1002/grl.50792, 2013. 34152

15 de Boer, G., Morrison, H., Shupe, M. D., and Hildner, R.: Evidence of liquid dependent ice nucleation in high-latitude stratiform clouds from surface remote sensors, Geophys. Res. Lett., 38, L01803, doi:10.1029/2010GL046016, 2011. 34151

20 DeMott, P. J., Prenni, A. J., Liu, X., Kreidenweis, S. M., Petters, M. D., Twohy, C. H., Richardson, M. S., Eidhammer, T., and Rogers, D. C.: Predicting global atmospheric ice nuclei distributions and their impacts on climate, P. Natl. Acad. Sci. USA, 107, 11217–11222, doi:10.1073/pnas.0910818107, 2010. 34151, 34157, 34159, 34163, 34164, 34165, 34174, 34175, 34193, 34201

25 DeMott, P. J., Prenni, A. J., McMeeking, G. R., Sullivan, R. C., Petters, M. D., Tobo, Y., Niemann, M., Möhler, O., Snider, J. R., Wang, Z., and Kreidenweis, S. M.: Integrating laboratory and field data to quantify the immersion freezing ice nucleation activity of mineral dust particles, Atmos. Chem. Phys., 15, 393–409, doi:10.5194/acp-15-393-2015, 2015. 34151, 34157, 34159, 34163, 34164, 34165, 34174, 34175, 34193, 34201

30 Deng, Z. Z., Zhao, C. S., Ma, N., Liu, P. F., Ran, L., Xu, W. Y., Chen, J., Liang, Z., Liang, S., Huang, M. Y., Ma, X. C., Zhang, Q., Quan, J. N., Yan, P., Henning, S., Mildenberger, K., Sommerhage, E., Schäfer, M., Stratmann, F., and Wiedensohler, A.: Size-resolved and bulk activation properties of aerosols in the North China Plain, Atmos. Chem. Phys., 11, 3835–3846, doi:10.5194/acp-11-3835-2011, 2011. 34151, 34163

- Ditas, F., Shaw, R. A., Siebert, H., Simmel, M., Wehner, B., and Wiedensohler, A.: Aerosols-cloud microphysics-thermodynamics-turbulence: evaluating supersaturation in a marine stratuscumulus cloud, *Atmos. Chem. Phys.*, 12, 2459–2468, doi:10.5194/acp-12-2459-2012, 2012. 34163
- 5 Dubovik, O. and King, M.: A flexible inversion algorithm for retrieval of aerosol optical properties from sun and sky radiance measurements, *J. Geophys. Res.*, 105, 20673–20696, doi:10.1029/2000JD900282, 2000. 34156, 34157
- 10 Dubovik, O., Sinyuk, A., Lapyonok, T., Holben, B. N., Mishchenko, M., Yang, P., Eck, T. F., Voltne, H., Munoz, O., Veihelmann, B., Van der Zande, W. J., Leon, J.-F., Sorokin, M., and Slutsker, I.: Application of spheroid models to account for aerosol particle nonsphericity in remote sensing of desert dust, *J. Geophys. Res.*, 111, D11208, doi:10.1029/2005JD006619, 2006. 34156, 34157
- 15 Ebert, M., Worringen, A., Benker, N., Mertes, S., Weingartner, E., and Weinbruch, S.: Chemical composition and mixing-state of ice residuals sampled within mixed phase clouds, *Atmos. Chem. Phys.*, 11, 2805–2816, doi:10.5194/acp-11-2805-2011, 2011. 34152
- 20 Engelmann, R., Kanitz, T., Baars, H., Heese, B., Althausen, D., Skupin, A., Wandinger, U., Komppula, M., Stachlewska, I. S., Amiridis, V., Marinou, E., Mattis, I., Linné, H., and Ansmann, A.: EARLINET Raman Lidar Polly^{XT}: the neXT generation, *Atmos. Meas. Tech. Discuss.*, 8, 7737–7780, doi:10.5194/amtd-8-7737-2015, 2015. 34158, 34161
- 25 Freudenthaler, V., Esselborn, M., Wiegner, M., Heese, B., Tesche, M., Ansmann, A., Müller, D., Althausen, D., Wirth, M., Fix, A., Ehret, G., Knippertz, P., Toledano, C., Gasteiger, J., Garhammer, M., and Seefeldner, M.: Depolarization ratio profiling at several wavelengths in pure Saharan dust during SAMUM 2006, *Tellus B*, 61, 165–179, doi:10.1111/j.1600-0889.2008.00396.x, 2009. 34153
- 30 Ghan, S. J. and Collins, D. R.: Use of In situ data to test a raman lidar-based cloud condensation nuclei remote sensing method, *J. Atmos. Ocean. Tech.*, 21, 387–394, doi:10.1175/1520-0426(2004)021<0387:UOISDT>2.0.CO;2, 2004. 34152
- Ghan, S. J., Rissman, T. A., Elleman, R., Ferrare, R. A., Turner, D., Flynn, C., Wang, J., Ogren, J., Hudson, J., Jonsson, H. H., VanReken, T., Flagan, R. C., and Seinfeld, J. H.: Use of in situ cloud condensation nuclei, extinction, and aerosol size distribution measurements to test a method for retrieving cloud condensation nuclei profiles from surface measurements, *J. Geophys. Res.*, 111, D05S10, doi:10.1029/2004JD005752, 2006. 34152

Lidar profiling of CCN- and INP-relevant aerosol parameters

R. E. Mamouri and
A. Ansmann

[Title Page](#)

[Abstract](#) [Introduction](#)

[Conclusions](#) [References](#)

[Tables](#) [Figures](#)

◀

▶

◀

▶

[Back](#)

[Close](#)

[Full Screen / Esc](#)

[Printer-friendly Version](#)

[Interactive Discussion](#)



- Granados-Muñoz, M. J., Bravo-Aranda, J. A., Baumgardner, D., Guerrero-Rascado, J. L., Pérez-Ramírez, D., Navas-Guzmán, F., Veselovskii, I., Lyamani, H., Valenzuela, A., Olmo, F. J., Titos, G., Andrey, J., Chaikovsky, A., Dubovik, O., Gil-Ojeda, M., and Alados-Arboledas, L.: Study of aerosol microphysical properties profiles retrieved from ground-based remote sensing and aircraft in-situ measurements during a Saharan dust event, *Atmos. Meas. Tech. Discuss.*, 8, 9289–9338, doi:10.5194/amtd-8-9289-2015, 2015. 34158
- Groß, S., Tesche, M., Freudenthaler, V., Toledano, C., Wiegner, M., Ansmann, A., Althausen, D., and Seefeldner, M.: Characterization of Saharan dust, marine aerosols and mixtures of biomass-burning aerosols and dust by means of multi-wavelength depolarization and Raman lidar measurements during SAMUM 2, *Tellus B*, 63, 706–724, doi:10.1111/j.1600-0889.2011.00556.x, 2011. 34160
- Groß, S., Esselborn, M., Weinzierl, B., Wirth, M., Fix, A., and Petzold, A.: Aerosol classification by airborne high spectral resolution lidar observations, *Atmos. Chem. Phys.*, 13, 2487–2505, doi:10.5194/acp-13-2487-2013, 2013. 34161
- Groß, S., Freudenthaler, V., Schepanski, K., Toledano, C., Schäfler, A., Ansmann, A., and Weinzierl, B.: Characterization of long-range transported Saharan dust at the Caribbean by dual-wavelength depolarization Raman lidar measurements, *Atmos. Chem. Phys. Discuss.*, 15, 19325–19366, doi:10.5194/acpd-15-19325-2015, 2015. 34156
- Haarig, M., Althausen, D., Ansmann, A., Klepel, A., Baars, H., Engelmann, R., Groß, S., and Freudenthaler, V.: Measurement of the linear depolarization ratio of aged dust at three wavelengths (355, 532 and 1064 nm) simultaneously over Barbados, in: Proceedings of the 27th International Laser Radar Conference, New York City, 5–10 July 2015, S8b.04, 2015. 34156
- Hartmann, S., Augustin, S., Clauss, T., Wex, H., Šantl-Temkiv, T., Voigtlander, J., Niedermeyer, D., and Stratmann, F.: Immersion freezing of ice nucleation active protein complexes, *Atmos. Chem. Phys.*, 13, 5751–5766, doi:10.5194/acp-13-5751-2013, 2013. 34152
- Henning, S., Dieckmann, K., Ignatius, K., Schäfer, M., Zedler, P., Harris, E., Sinha, B., van Pinxteren, D., Mertes, S., Birmili, W., Merkel, M., Wu, Z., Wiedensohler, A., Wex, H., Herrmann, H., and Stratmann, F.: Influence of cloud processing on CCN activation behaviour in the Thuringian Forest, Germany during HCCT-2010, *Atmos. Chem. Phys.*, 14, 7859–7868, doi:10.5194/acp-14-7859-2014, 2014. 34163
- Hiranuma, N., Kohn, M., Pekour, M. S., Nelson, D. A., Shilling, J. E., and Cziczo, D. J.: Droplet activation, separation, and compositional analysis: laboratory studies and atmospheric measurements, *Atmos. Meas. Tech.*, 4, 2333–2343, doi:10.5194/amt-4-2333-2011, 2011. 34163

Lidar profiling of CCN- and INP-relevant aerosol parameters

R. E. Mamouri and
A. Ansmann

[Title Page](#)

[Abstract](#)

[Introduction](#)

[Conclusions](#)

[References](#)

[Tables](#)

[Figures](#)

[|◀](#)

[▶|](#)

[◀](#)

[▶](#)

[Back](#)

[Close](#)

[Full Screen / Esc](#)

[Printer-friendly Version](#)

[Interactive Discussion](#)



Holben, B. N., Eck, T. F., Slutsker, I., Tanré, D., Buis, J. P., Setzer, A., Vermote, E., Reagan, J. A., Kaufman, Y. J., Nakajima, T., Lavenu, F., Jankowiak, I., and Smirnov, A.: AERONET – a federated instrument network and data archive for aerosol characterization, *Remote Sens. Environ.*, 66, 1–16, 1998. 34154

5 Illingworth, A. J., Hogan, R. J., O'Connor, E. J., Bouniol, D., Delanoe, J., Pelon, J., Protat, A., Brooks, M. E., Gaussiat, N., Wilson, D. R., Donovan, D. P., Klein Baltink, H., van Zadelhoff, G.-J., Eastment, J. D., Goddard, J. W. F., Wrench, C. L., Haeflalin, M., Krasnov, O. A., Russchenberg, H. W. J., Piriou, J.-M., Vinit, F., Seifert, A., Tompkins, A. M., and Willen, J., CLOUDNET: continuos evaluation of cloud profiles in seven operational models using ground-based observations, *B. Am. Meteorol. Soc.*, 88, 883–898, 2007. 34151

10 Illingworth, A. J., Barker, H. W., Beljaars, A., Ceccaldi, M., Chepfer, H., Clerbaux, N., Cole, J., Delanoe, J., Domenech, C., Donovan, D. P., Fukuda, S., Hirakata, M., Hogan, R. J., Huenerbein, H., Kollias, P., Kubota, T., Nakajima, T., Nakajima, T. Y., Nishizawa, T., Ohno, Y., Okamoto, H., Oki, R., Sato, K., Satoh, M., Shephard, M., Velázquez-Blázquez, A., Wandinger, U., Wehr, T., and Zadelhoff, G.-J.: THE EARTHCARE SATELLITE: the next step forward in global measurements of clouds, aerosols, precipitation and radiation, *B. Am. Meteorol. Soc.*, 96, 1311–1332, doi:10.1175/BAMS-D-12-00227.1, 2015. 34153, 34174

15 IPCC 2013: Climate Change 2013: The Physical Science Basis. Contribution of Working Group I to the Fifth Assessment Report of the Intergovernmental Panel on Climate Change, edited by: Stocker, T. F., Qin, D., Plattner, G.-K., Tignor, M., Allen, S. K., Boschung, J., Nauels, A., Xia, Y., Bex, V., and Midgley, P. M., Cambridge University Press, Cambridge, UK and New York, NY, USA, 1535 pp., available at: http://www.climatechange2013.org/images/report/WG1AR5_ALL_FINAL.pdf (last access: 29 January 2014), 2013. 34151

20 Jefferson, A.: Empirical estimates of CCN from aerosol optical properties at four remote sites, *Atmos. Chem. Phys.*, 10, 6855–6861, doi:10.5194/acp-10-6855-2010, 2010. 34152

Ji, Q. and Shaw, G. E.: On supersaturation spectrum and size distributions of cloud condensation nuclei, *Geophys. Res. Lett.*, 25, 1903–1906, doi:10.1029/98GL01404, 1998. 34163

25 Kamphus, M., Ettner-Mahl, M., Klimach, T., Drewnick, F., Keller, L., Cziczo, D. J., Mertes, S., Borrmann, S., and Curtius, J.: Chemical composition of ambient aerosol, ice residues and cloud droplet residues in mixed-phase clouds: single particle analysis during the Cloud and Aerosol Characterization Experiment (CLACE 6), *Atmos. Chem. Phys.*, 10, 8077–8095, doi:10.5194/acp-10-8077-2010, 2010. 34152

Lidar profiling of CCN- and INP-relevant aerosol parameters

R. E. Mamouri and
A. Ansmann

[Title Page](#)

[Abstract](#)

[Introduction](#)

[Conclusions](#)

[References](#)

[Tables](#)

[Figures](#)

◀

▶

◀

▶

[Back](#)

[Close](#)

[Full Screen / Esc](#)

[Printer-friendly Version](#)

[Interactive Discussion](#)



- Kanitz, T., Seifert, P., Ansmann, A., Engelmann, R., Althausen, D., Casiccia, C., and Roher, E. G.: Contrasting the impact of aerosols at northern and southern midlatitudes on heterogeneous ice formation, *Geophys. Res. Lett.*, 38, L17802, doi:10.1029/2011GL048532, 2011. 34152
- 5 Kanitz, T., Engelmann, R., Heinold, B., Baars, H., Skupin, A., and Ansmann, A.: Tracking the Saharan Air Layer with shipborne lidar across the tropical Atlantic, *Geophys. Res. Lett.*, 41, 1044–1050, doi:10.1002/2013GL058780, 2014. 34161
- 10 Kolgotin, A., Korenskiy, M., and Veselovskii, I.: Direct estimation of fine and coarse mode particle parameters from multiwavelength lidar measurements, in: Proceedings of the 27th International Laser Radar Conference, New York City, 5–10 July 2015, SA5.10, 2015. 34170
- Liu, J. and Li, Z.: Estimation of cloud condensation nuclei concentration from aerosol optical quantities: influential factors and uncertainties, *Atmos. Chem. Phys.*, 14, 471–483, doi:10.5194/acp-14-471-2014, 2014. 34152, 34169
- 15 Mamouri, R. E. and Ansmann, A.: Fine and coarse dust separation with polarization lidar, *Atmos. Meas. Tech.*, 7, 3717–3735, doi:10.5194/amt-7-3717-2014, 2014. 34153, 34156, 34160, 34161
- Mamouri, R. E. and Ansmann, A.: Estimated desert-dust ice nuclei profiles from polarization lidar: methodology and case studies, *Atmos. Chem. Phys.*, 15, 3463–3477, doi:10.5194/acp-15-3463-2015, 2015. 34152, 34153, 34156, 34157, 34158, 34159, 34164, 34171, 34174, 20 34198
- Mamouri, R. E., Ansmann, A., Nisantzi, A., Kokkalis, P., Schwarz, A., and Hadjimitsis, D.: Low Arabian dust extinction-to-backscatter ratio, *Geophys. Res. Lett.*, 40, 4762–4766, doi:10.1002/grl.50898, 2013. 34153, 34158, 34160, 34161
- 25 Mattis, I., Ansmann, A., Müller, D., Wandinger, U., and Althausen, D.: Multiyear aerosol observations with dual-wavelength Raman lidar in the framework of EARLINET, *J. Geophys. Res.*, 109, D13203, doi:10.1029/2004JD004600, 2004. 34155, 34161, 34167
- Mattis, I., Müller, D., Ansmann, A., Wandinger, U., Preißler, J., Seifert, P., and Tesche, M.: Ten 30 years of multiwavelength Raman lidar observations of free-tropospheric aerosol layers over central Europe: geometrical properties and annual cycle, *J. Geophys. Res.*, 113, D20202, doi:10.1029/2007JD009636, 2008. 34155, 34167
- Müller, D., Mattis, I., Wandinger, U., Ansmann, A., Althausen, A., and Stohl, A.: Raman lidar observations of aged Siberian and Canadian forest fire smoke in the free troposphere over

Lidar profiling of CCN- and INP-relevant aerosol parameters

R. E. Mamouri and
A. Ansmann

[Title Page](#)

[Abstract](#)

[Introduction](#)

[Conclusions](#)

[References](#)

[Tables](#)

[Figures](#)

[|◀](#)

[▶|](#)

[◀](#)

[▶](#)

[Back](#)

[Close](#)

[Full Screen / Esc](#)

[Printer-friendly Version](#)

[Interactive Discussion](#)

Germany in 2003: microphysical particle characterization, *J. Geophys. Res.*, 110, D17201, doi:10.1029/2004JD005756, 2005. 34152

Müller, D., Ansmann, A., Mattis, I., Tesche, M., Wandinger, U., Althausen, D., and Pisani, G.: Aerosol-type-dependent lidar ratios observed with Raman lidar, *J. Geophys. Res.*, 112, D16202, doi:10.1029/2006JD008292, 2007. 34161

Müller, D., Veselovskii, I., Kolgotin, A., Tesche, M., Ansmann, A., and Dubovik, O.: Vertical profiles of pure dust and mixed smoke-dust plumes inferred from inversion of multiwavelength Raman/polarization lidar data and comparison to AERONET retrievals and in situ observations, *Appl. Optics*, 52, 3178–3202, doi:10.1364/AO.52.003178, 2013. 34152

Müller, D., Hostetler, C. A., Ferrare, R. A., Burton, S. P., Chemyakin, E., Kolgotin, A., Hair, J. W., Cook, A. L., Harper, D. B., Rogers, R. R., Hare, R. W., Cleckner, C. S., Oblean, M. D., Tomlinson, J., Berg, L. K., and Schmid, B.: Airborne Multiwavelength High Spectral Resolution Lidar (HSRL-2) observations during TCAP 2012: vertical profiles of optical and microphysical properties of a smoke/urban haze plume over the northeastern coast of the US, *Atmos. Meas. Tech.*, 7, 3487–3496, doi:10.5194/amt-7-3487-2014, 2014. 34152

Murray, B. J., O'Sullivan, D., Atkinson, J. D., and Webb, M. E.: Ice nucleation by particles immersed in supercooled cloud droplets, *Chem. Soc. Rev.*, 41, 6519–6554, doi:10.1039/c2cs35200a, 2012. 34152

Nakajima, T., Higurashi, A., Kawamoto, K., and Penner, J. E.: A possible correlation between satellite-derived cloud and aerosol microphysical parameters, *Geophys. Res. Lett.*, 28, 1171–1174, doi:10.1029/2000GL012186, 2001. 34169

Niemand, M., Möhler, O., Vogel, B., Vogel, H., Hoose, C., Connolly, P., Klein, H., Bingemer, H., DeMott, P., Skrotzki, J., and Leisner, T.: Parameterization of immersion freezing on mineral dust particles: an application in a regional scale model, *J. Atmos. Sci.*, 69, 3077–3092, 2012. 34151, 34153, 34159, 34163, 34165, 34174, 34175, 34193, 34201

Nisantzi, A., Mamouri, R. E., Ansmann, A., and Hadjimitsis, D.: Injection of mineral dust into the free troposphere during fire events observed with polarization lidar at Limassol, Cyprus, *Atmos. Chem. Phys.*, 14, 12155–12165, doi:10.5194/acp-14-12155-2014, 2014. 34153, 34167

Nisantzi, A., Mamouri, R. E., Ansmann, A., Schuster, G. L., and Hadjimitsis, D. G.: Middle East versus Saharan dust extinction-to-backscatter ratios, *Atmos. Chem. Phys.*, 15, 7071–7084, doi:10.5194/acp-15-7071-2015, 2015. 34153, 34155, 34156, 34158, 34160, 34167

Papayannis, A., Amiridis, V., Mona, L., Tsaknakis, G., Balis, D., Bösenberg, J., Chaikovski, A., De Tomasi, F., Grigorov, I., Mattis, I., Mitev, V., Müller, D., Nickovic, S., Pérez, C.,

Lidar profiling of CCN- and INP-relevant aerosol parameters

R. E. Mamouri and
A. Ansmann

[Title Page](#)

[Abstract](#)

[Introduction](#)

[Conclusions](#)

[References](#)

[Tables](#)

[Figures](#)

[◀](#)

[▶](#)

[Back](#)

[Close](#)

[Full Screen / Esc](#)

[Printer-friendly Version](#)

[Interactive Discussion](#)



- Pietruczuk, A., Pisani, G., Ravetta, F., Rizi, V., Sicard, M., Trickl, T., Wiegner, M., Gerding, M., Mamouri, R. E., D'Amico, G., and Pappalardo, G.: Systematic lidar observations of Saharan dust over Europe in the frame of EARLINET (2000–2002), *J. Geophys. Res.*, 113, D10204, doi:10.1029/2007JD009028, 2008. 34167
- 5 Pappalardo, G., Amodeo, A., Apituley, A., Comeron, A., Freudenthaler, V., Linné, H., Ansmann, A., Bösenberg, J., D'Amico, G., Mattis, I., Mona, L., Wandinger, U., Amiridis, V., Alados-Arboledas, L., Nicolae, D., and Wiegner, M.: EARLINET: towards an advanced sustainable European aerosol lidar network, *Atmos. Meas. Tech.*, 7, 2389–2409, doi:10.5194/amt-7-2389-2014, 2014. 34158
- 10 Prospero, J. M. and Mayol-Bracero, O. L.: Understanding the transport and impact of African dust on the Caribbean Basin, *B. Am. Meteorol. Soc.*, 94, 1329–1337, doi:10.1175/BAMS-D-12-00142.1, 2013. 34156
- 15 Pummer, B. G., Budke, C., Augustin-Bauditz, S., Niedermeier, D., Felgitsch, L., Kampf, C. J., Huber, R. G., Liedl, K. R., Loerting, T., Moschen, T., Schauperl, M., Tollinger, M., Morris, C. E., Wex, H., Grothe, H., Pöschl, U., Koop, T., and Fröhlich-Nowoisky, J.: Ice nucleation by water-soluble macromolecules, *Atmos. Chem. Phys.*, 15, 4077–4091, doi:10.5194/acp-15-4077-2015, 2015. 34152
- 20 Quinn, P. K., Bates, T. S., Coffman, D. J., and Covert, D. S.: Influence of particle size and chemistry on the cloud nucleating properties of aerosols, *Atmos. Chem. Phys.*, 8, 1029–1042, doi:10.5194/acp-8-1029-2008, 2008. 34151, 34163
- 25 Rose, D., Nowak, A., Achtert, P., Wiedensohler, A., Hu, M., Shao, M., Zhang, Y., Andreae, M. O., and Pöschl, U.: Cloud condensation nuclei in polluted air and biomass burning smoke near the mega-city Guangzhou, China – Part 1: Size-resolved measurements and implications for the modeling of aerosol particle hygroscopicity and CCN activity, *Atmos. Chem. Phys.*, 10, 3365–3383, doi:10.5194/acp-10-3365-2010, 2010. 34151, 34163
- 30 Schmidt, J., Ansmann, A., Bühl, J., Baars, H., Wandinger, U., Müller, D., and Malinka, A. V.: Dual-FOV Raman and Doppler lidar studies of aerosol-cloud interactions: simultaneous profiling of aerosols, warm-cloud properties, and vertical wind, *J. Geophys. Res.*, 119, 5512–5527, doi:10.1002/2013JD020424, 2014. 34151, 34176
- 35 Seifert, P., Ansmann, A., Mattis, I., Wandinger, U., Tesche, M., Engelmann, R., Müller, D., Pérez, C., and Haustein, K.: Saharan dust and heterogeneous ice formation: eleven years of cloud observations at a central European EARLINET site, *J. Geophys. Res.*, 115, D20201, doi:10.1029/2009JD013222, 2010. 34152

Title Page	
Abstract	Introduction
Conclusions	References
Tables	Figures
◀	▶
◀	▶
Back	Close
Full Screen / Esc	
Printer-friendly Version	
Interactive Discussion	

- Shinozuka, Y., Clarke, A. D., Nenes, A., Jefferson, A., Wood, R., McNaughton, C. S., Ström, J., Tunved, P., Redemann, J., Thornhill, K. L., Moore, R. H., Lathem, T. L., Lin, J. J., and Yoon, Y. J.: The relationship between cloud condensation nuclei (CCN) concentration and light extinction of dried particles: indications of underlying aerosol processes and implications for satellite-based CCN estimates, *Atmos. Chem. Phys.*, 15, 7585–7604, doi:10.5194/acp-15-7585-2015, 2015. 34152, 34161, 34163, 34166, 34168, 34169, 34173
- Shupe, M. D.: A ground-based multisensor cloud phase classifier, *Geophys. Res. Lett.*, 34, L22809, doi:10.1029/2007GL031008, 2007. 34151
- Siebert, H., Beals, M., Bethke, J., Bierwirth, E., Conrath, T., Dieckmann, K., Ditas, F., Ehrlich, A., Farrell, D., Hartmann, S., Izaguirre, M. A., Katzwinkel, J., Nuijens, L., Roberts, G., Schäfer, M., Shaw, R. A., Schmeissner, T., Serikov, I., Stevens, B., Stratmann, F., Wehner, B., Wendisch, M., Werner, F., and Wex, H.: The fine-scale structure of the trade wind cumuli over Barbados – an introduction to the CARRIBA project, *Atmos. Chem. Phys.*, 13, 10061–10077, doi:10.5194/acp-13-10061-2013, 2013. 34163
- Steinke, I., Hoose, C., Möhler, O., Connolly, P., and Leisner, T.: A new temperature- and humidity-dependent surface site density approach for deposition ice nucleation, *Atmos. Chem. Phys.*, 15, 3703–3717, doi:10.5194/acp-15-3703-2015, 2015. 34151, 34153, 34159, 34163, 34165, 34166, 34174, 34175, 34193, 34201
- Tesche, M., Ansmann, A., Müller, D., Althausen, D., Engelmann, R., Freudenthaler, V., and Groß, S.: Vertically resolved separation of dust and smoke over Cape Verde using multi-wavelength Raman and polarization lidars during Saharan Mineral Dust Experiment 2008, *J. Geophys. Res.*, 114, D13202, doi:10.1029/2009JD011862, 2009. 34153, 34156, 34160, 34161
- Tesche, M., Groß, S., Ansmann, A., Müller, D., Althausen, D., Freudenthaler, V., and Eselborn, M.: Profiling of Saharan dust and biomass-burning smoke with multiwavelength polarization Raman lidar at Cape Verde, *Tellus B*, 63, 649–676, doi:10.1111/j.1600-0889.2011.00548.x, 2011. 34153, 34156
- Toledano, C., Wiegner, M., Garhammer, M., Seefeldner, M., Gasteiger, J., Müller, D., and Koepke, P.: Spectral aerosol optical depth characterization of desert dust during SAMUM 2006, *Tellus B*, 61, 216–228, doi:10.1111/j.1600-0889.2008.00382.x, 2009. 34155, 34156
- Toledano, C., Wiegner, M., Groß, S., Freudenthaler, V., Gasteiger, J., Müller, D., Müller, T., Schladitz, A., Weinzierl, B., Torres, B., and O'Neill, N. T.: Optical properties of aerosol

Discussion Paper | Discussion Paper

Lidar profiling of CCN- and INP-relevant aerosol parameters

R. E. Mamouri and
A. Ansmann

[Title Page](#)[Abstract](#)[Introduction](#)[Conclusions](#)[References](#)[Tables](#)[Figures](#)[|◀](#)[▶|](#)[Back](#)[Close](#)[Full Screen / Esc](#)[Printer-friendly Version](#)[Interactive Discussion](#)

Lidar profiling of CCN- and INP-relevant aerosol parameters

R. E. Mamouri and
A. Ansmann

- mixtures derived from sun-sky radiometry during SAMUM-2, Tellus B, 63, 635–648, doi:10.1111/j.1600-0889.2011.00573.x, 2011. 34155, 34156
- Umo, N. S., Murray, B. J., Baeza-Romero, M. T., Jones, J. M., Lea-Langton, A. R., Malkin, T. L., O'Sullivan, D., Neve, L., Plane, J. M. C., and Williams, A.: Ice nucleation by combustion ash particles at conditions relevant to mixed-phase clouds, *Atmos. Chem. Phys.*, 15, 5195–5210, doi:10.5194/acp-15-5195-2015, 2015. 34152
- Veselovskii, I., Dubovik, O., Kolgotin, A., Lapyonok, T., Di Girolamo, P., Summa, D., Whiteman, D. N., Mishchenko, M., and Tanr'e, D.: Application of randomly oriented spheroids for retrieval of dust particle parameters from multiwavelength lidar measurements, *J. Geophys. Res.*, 115, D21203, doi:10.1029/2010JD014139, 2010. 34152
- Wandinger, U., Mattis, I., Tesche, M., Ansmann, A., Bösenberg, J., Chaikovski, A., Freudenthaler, V., Komguem, L., Linné, H., Matthias, V., Pelon, J., Sauvage, L., Sobolewski, P., Vaughan, G., and Wiegner, M.: Air mass modification over Europe: EARLINET aerosol observations from Wales to Belarus, *J. Geophys. Res.*, 109, D24205, doi:10.1029/2004JD005142, 2004. 34167
- Weinzierl, B., Petzold, A., Esselborn, M., Wirth, M., Rasp, K., Kandler, K., Schütz, L., Koepke, P., and Fiebig, M.: Airborne measurements of dust layer properties, particle size distribution and mixing state of Saharan dust during SAMUM 2006, *Tellus B*, 61, 96–117, doi:10.1111/j.1600-0889.2008.00392.x, 2009. 34163
- Wex, H., DeMott, P. J., Tobo, Y., Hartmann, S., Rösch, M., Clauss, T., Tomsche, L., Niedermeier, D., and Stratmann, F.: Kaolinite particles as ice nuclei: learning from the use of different kaolinite samples and different coatings, *Atmos. Chem. Phys.*, 14, 5529–5546, doi:10.5194/acp-14-5529-2014, 2014. 34165
- Wiegner, M. and Geiß, A.: Aerosol profiling with the Jenoptik ceilometer CHM15kx, *Atmos. Meas. Tech.*, 5, 1953–1964, doi:10.5194/amt-5-1953-2012, 2012. 34153
- Wiegner, M., Madonna, F., Binietoglou, I., Forkel, R., Gasteiger, J., Geiß, A., Pappalardo, G., Schäfer, K., and Thomas, W.: What is the benefit of ceilometers for aerosol remote sensing? An answer from EARLINET, *Atmos. Meas. Tech.*, 7, 1979–1997, doi:10.5194/amt-7-1979-2014, 2014. 34153
- Zhang, D., Wang, Z., and Liu, D.: A global view of midlevel liquid-layer topped stratiform cloud distribution and phase partition from CALIPSO and CloudSat measurements, *J. Geophys. Res.*, 115, D00H13, doi:10.1029/2009JD012143, 2010. 34152

Title Page

Abstract

Introduction

Conclusions

References

Tables

Figures

|◀

▶|

◀

▶

Back

Close

Full Screen / Esc

Printer-friendly Version

Interactive Discussion



Table 1. Available AERONET data sets (optical as well as microphysical properties of aerosol particles) for the three defined basic aerosol types. A total number of 48 474 observation were taken at Limassol during the 2011–2015 time period, 1745 level-2.0 out of 4190 measurements (level 1.5) of the particle size distribution are available in the AERONET data base from which APC and ASC values could be calculated. A total number of 34 982 level 1.5 observations were taken at Leipzig from 2001–2015. 4651 measurements (level 1.5) with size distributions are available. 118 data sets of optical properties and inverted particle size distributions are available from the field campaigns (SAMUM, SALTRACE). 123 respective Ragged Point observations (Barbados) for pure marine conditions could be analyzed for our study. AE denotes Ångström exponent. CIMH stands for Caribbean Institute for Meteorology and Hydrology.

Site	Observational period	Number of obs.	Dominating aerosol type
Limassol, Cyprus (CUT-TEPAK, 34.7° N, 33.0° E, 25 m.a.s.l.)	July 2011–June 2015	421	cont. pollution, AE > 1.6
		134	mineral dust, AE < 0.5
Leipzig, Germany (TROPOS, 51.4° N, 12.4° E, 125 m.a.s.l.)	May 2001–June 2015	1912	cont. pollution, AE > 1.6
		124	mineral dust, AE < 0.5
Ouarazate, Morocco (SAMUM-1, 30.9° N, 6.9° W, 1150 m.a.s.l.)	May–June 2006	32	mineral dust
Praia, Cabo Verde (SAMUM-2, 14.9° N, 23.4° W, 70 m.a.s.l.)	January 2008	9	mineral dust
Barbados (SALTRACE-1, CIMH, 13.1° N, 59.6° W, 110 m.a.s.l.)	June–July 2013	22	mineral dust
Barbados (SALTRACE-3, Ragged Point, 13.2° N, 59.4° W, 40 m.a.s.l.)	June–July 2014	55	mineral dust
Barbados (Ragged Point)	August 2007–February 2015	123	marine aerosol

Title Page

Abstract

Introduction

Conclusions

References

Tables

Figures

|◀

▶|

◀

▶

Back

Close

Full Screen / Esc

Printer-friendly Version

Interactive Discussion



Lidar profiling of CCN- and INP-relevant aerosol parameters

R. E. Mamouri and
A. Ansmann

Table 2. Overview of the data analysis from the basic lidar-derived aerosol optical properties (backscatter and extinction (AEC) coefficients) to the height profiles of the CCNC proxy $\text{APC}_{\text{CCN},s}$ and INPC. Index s denotes supersaturation with respect to liquid water. Indices m, c, d stand for marine aerosol, continental fine-mode-dominated pollution (anthropogenic haze, biomass burning smoke, other continental non-dust contributions), and mineral dust, respectively.

Step	Computed parameters	Equation terms
1	Profiles of particle backscatter coefficient and particle linear depolarization ratio	β_p, δ_p
2	Separation of dust and non-dust backscatter coefficients	β_d, β_{nd}
3	Conversion to dust, marine and continental pollution AEC profiles	$\sigma_d, \sigma_m, \sigma_c$
4	Conversion of AEC to profiles of APC_{50} , APC_{250} , and ASC for each aerosol type i	$n_{P50,i}, n_{P250,i}, s_{P,i}$
5	Estimation of $\text{APC}_{\text{CCN},s}$ with APC_{50} as input	$n_{\text{CCN},s,i}$
6	Estimation of INPC profiles with APC_{250} and ASC as input	$n_{\text{INP},i}$

[Title Page](#)[Abstract](#)[Introduction](#)[Conclusions](#)[References](#)[Tables](#)[Figures](#)[|◀](#)[▶|](#)[Back](#)[Close](#)[Full Screen / Esc](#)[Printer-friendly Version](#)[Interactive Discussion](#)

Table 3. Parameters $c_{P50,i}$, $c_{P250,i}$, and $c_{PS,i}$ and aerosol extinction exponent x_i required in the conversion of particle extinction coefficients into particle number and surface area concentrations with Eqs. (1)–(3) in Sect. 3.2. Values are given for the laser wavelengths of 355 (380 nm), 532, and 1064 nm. $c_{P50,i}$ and x_i and respective standard deviations are obtained from the regression analysis. The mean values and standard deviation of $c_{P250,i}$, and $c_{PS,i}$ are computed from averaging of all individual observations of a given data set. In the case of Limassol and Leipzig data, all observations with $\text{AE} (440\text{--}870 \text{ nm}) > 1.6$ are interpreted as continental-pollution-dominated cases, and the observations with $\text{AE} (440\text{--}870 \text{ nm}) < 0.5$ are assumed to be dust-dominated. During SAMUM-1 the 340 nm channel of the AERONET photometer was not working properly. The same was true for Barbados photometers in 2014 so that we provide the respective values for 380 nm.

Location, aerosol, wavelength	$C_{P50,i}$ (Mm cm^{-3})	x_i	$C_{P250,i}$ (Mm cm^{-3})	$(10^{-12} \text{ Mm m}^2 \text{ cm}^{-3})$
Morocco, C. Verde, Barbados, dust, 380 nm	15.1	0.95 ± 0.11	0.18 ± 0.02	2.20 ± 0.47
Morocco, C. Verde, Barbados, dust, 532 nm	18.1	0.92 ± 0.11	0.19 ± 0.02	2.28 ± 0.51
Morocco, C. Verde, Barbados, dust, 1064 nm	28.8	0.85 ± 0.11	0.22 ± 0.03	2.65 ± 0.63
Cyprus, dust, 355 nm	13.7	1.05 ± 0.07	0.16 ± 0.03	2.60 ± 0.55
Cyprus, dust, 532 nm	20.3	1.00 ± 0.08	0.18 ± 0.03	2.90 ± 0.61
Cyprus, dust, 1064 nm	36.6	0.93 ± 0.07	0.23 ± 0.05	3.65 ± 0.85
Germany, dust, 355 nm	1.46	1.32 ± 0.07	0.18 ± 0.04	1.91 ± 0.53
Germany, dust, 532 nm	3.60	1.19 ± 0.06	0.21 ± 0.04	2.25 ± 0.59
Germany, dust, 1064 nm	12.2	1.00 ± 0.06	0.28 ± 0.17	2.88 ± 1.13
Cyprus, continental pollution, 355 nm	109.0	0.67 ± 0.04	0.10 ± 0.03	2.92 ± 0.97
Cyprus, continental pollution, 532 nm	108.5	0.75 ± 0.05	0.18 ± 0.04	5.15 ± 1.64
Cyprus, continental pollution, 1064 nm	484.0	0.60 ± 0.04	0.63 ± 0.20	18.01 ± 6.89
Germany, continental pollution, 355 nm	17.1	0.93 ± 0.02	0.12 ± 0.05	2.15 ± 0.70
Germany, continental pollution, 532 nm	35.0	0.90 ± 0.02	0.21 ± 0.08	3.92 ± 1.35
Germany, continental pollution, 1064 nm	176.4	0.76 ± 0.02	0.69 ± 0.34	12.93 ± 5.67
Barbados, marine, 355 nm	7.23	1.23 ± 0.15	0.18 ± 0.04	2.06 ± 0.34
Barbados, marine, 532 nm	10.6	1.00 ± 0.14	0.22 ± 0.04	2.51 ± 0.41
Barbados, marine, 1064 nm	35.9	0.77 ± 0.12	0.34 ± 0.11	3.78 ± 0.87

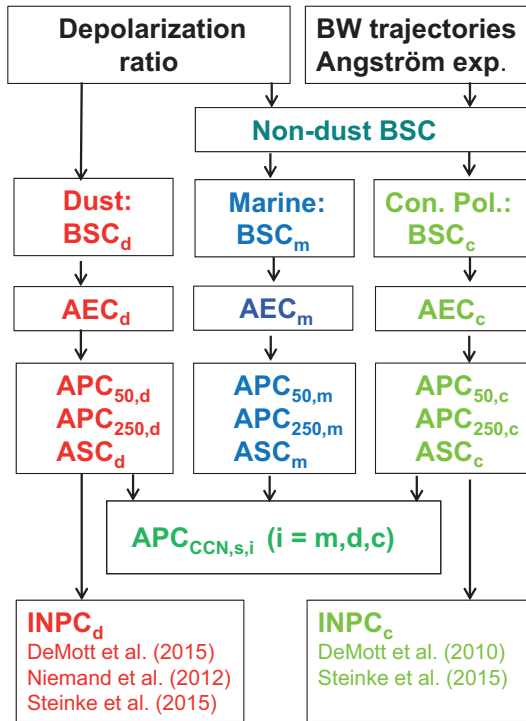


Figure 1. Sketch showing the way from basic lidar-derived dust and non-dust backscatter coefficients (BSC) to the separation of the extinction (AEC) contributions by different aerosol types, which are identified by means of, i.e., backward (BW) trajectory analysis and Ångström exponent information from lidar or AERONET observations. The aerosol-type-dependent AEC profiles are then converted to profiles of APC_{50} , APC_{250} , and ASC separately for each aerosol type (m, d, c). Finally $APC_{CCN,s}$ is estimated for a given supersaturation s as well as INPC profiles for mineral dust and continental aerosol pollution by applying parameterizations from the literature (DeMott et al., 2010, 2015; Niemand et al., 2012; Steinke et al., 2015).

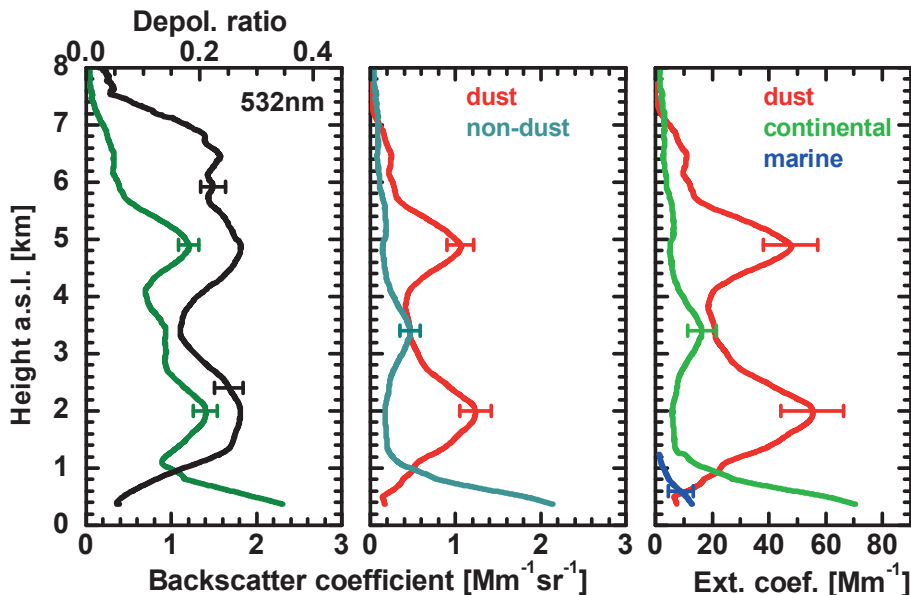


Figure 2. (Left) 532 nm particle backscatter coefficient (green) and particle linear depolarization ratio (black) as function of height above sea level (a.s.l.), (center) derived particle backscatter coefficients separately for non-dust (marine and anthropogenic aerosol, blue-green) and dust particles (red), and (right) particle extinction coefficients separately for marine (blue), anthropogenic pollution (green) and dust particles (red). Error bars indicate typical uncertainties. The observation was taken at Nicosia, Cyprus, during a desert dust outbreak from the Sahara on 7 April 2015. Mean profiles for the time period from 20:30–21:30 UTC are shown. The sum of the three extinction profiles match the Raman-lidar-derived total particle extinction profile. Lidar ratios used in the backscatter-to-extinction conversion are 45 sr for desert dust, 35 sr for anthropogenic haze, 20 sr for marine particles in the boundary layer.

Lidar profiling of CCN- and IP-relevant aerosol parameters

R. E. Mamouri and
A. Ansmann

Title Page

Abstract

Introduction

Conclusions

References

Tables

Figures

Tables

Figures

Tables

Tables

Figures

1

1

◀

▶

Back

Close

Full Screen / Esc

Printer friendly Version

Interactive Discussion



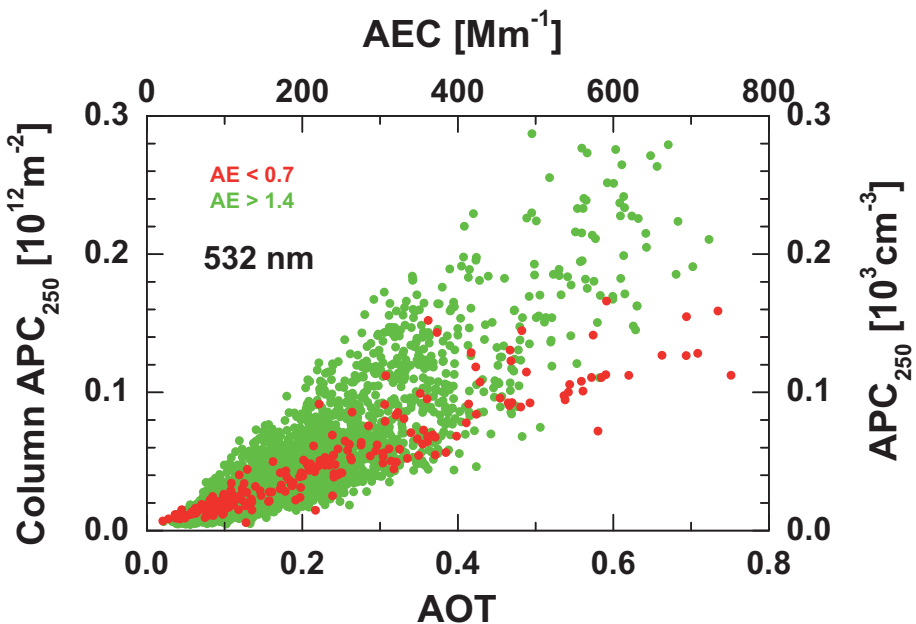


Figure 3. Replacement of the column-integrals (column APC₂₅₀, AOT) from the AERONET observations by volume-related quantities (APC₂₅₀, AEC) by assuming an arbitrarily chosen vertical height of the column of 1000 m. In this example, green symbols show all 3021 pollution-dominated Leipzig AERONET observations (2001–2015) with high Ångström exponent (AE > 1.4), and red symbols all 224 dust-dominated cases (AE < 0.7).

DISCUSSION ABCI

1
ape

Disc

卷二

-

卷之二

Title Page	
Abstract	Introduction
Conclusions	References
Tables	Figures
◀	▶
◀	▶
Back	Close
Full Screen / Esc	

[Printer-friendly Version](#)

Lidar profiling of CCN- and INP-relevant aerosol parameters

R. E. Mamouri and
A. Ansmann

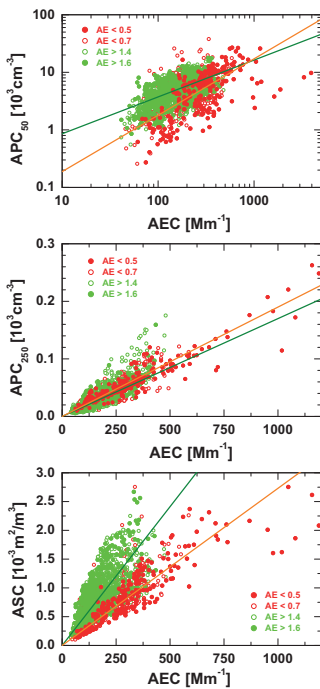


Figure 4. Particle number concentrations APC_{50} (all optically active particles, top) and APC_{250} (particles with radius $> 250 \text{ nm}$, center), and surface area concentration ASC (bottom) vs. 532 nm particle extinction coefficient AEC . AERONET observations (level 2.0) performed at Limassol, Cyprus, from 1 July 2011 to 30 June 2015 are shown. 839, 421, 213, and 134 level-2.0 observations are available at Ångström exponents of $\text{AE} > 1.4$ (open green circles), > 1.6 (solid green circles), < 0.7 (open red circles), and < 0.5 (solid red circles), respectively. The olive lines (fits to the data for $\text{AE} > 1.6$) and orange lines (fits to the data for $\text{AE} < 0.5$) indicate the mean increase of $\log \text{APC}_{50}$ with $\log \text{AEC}$ (532 nm, top panel), and the mean increase of APC_{250} and ASC with 532 nm AEC .

[Title Page](#)

[Abstract](#)

[Introduction](#)

[Conclusions](#)

[References](#)

[Tables](#)

[Figures](#)

◀

▶

◀

▶

[Back](#)

[Close](#)

[Full Screen / Esc](#)

[Printer-friendly Version](#)

[Interactive Discussion](#)

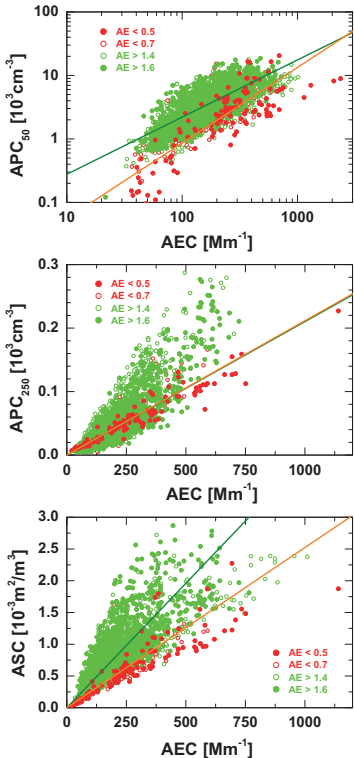
Lidar profiling of CCN- and INP-relevant aerosol parametersR. E. Mamouri and
A. Ansmann

Figure 5. Same as Fig. 4, except for the AERONET observations at Leipzig from 1 May 2001 and 30 June 2015. 4651 individual retrievals of the particle size distribution and thus of APC and ASC values are available for the 14 year period. 3022, 1912, 225, and 124 observations were taken at Ångström exponents of AE > 1.4 (open green circles), > 1.6 (solid green circles), < 0.7 (open red circles), and < 0.5 (solid red circles), respectively.

Lidar profiling of CCN- and INP-relevant aerosol parameters

R. E. Mamouri and
A. Ansmann

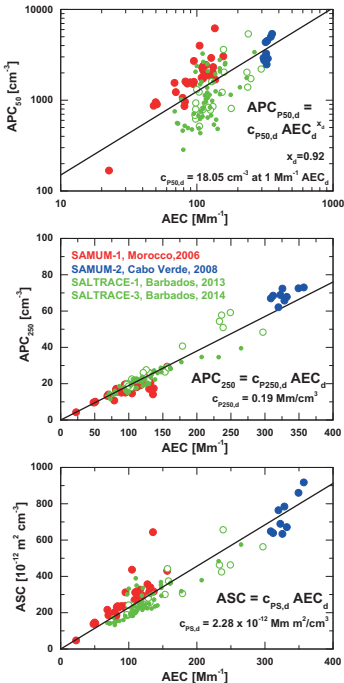


Figure 6. Relationship between dust layer mean 532 nm extinction coefficient AEC and dust layer mean APC_{50} (top), APC_{250} (center), and ASC (bottom) for observations taken during the desert dust field campaigns at Morocco (red, SAMUM-1, 2006), Cape Verde (blue, SAMUM-2, 2008), and Barbados (open green circles, SALTRACE-1, 2013, solid green circles, SALTRACE-3, 2014). The slope of the black lines are obtained in the same way as in Figs. 4 and 5. Note again, that the APC_{250}/AEC conversion factor is 0.19 and not 0.67 Mm^{-3} as erroneously given in Mamouri and Ansmann (2015).

Lidar profiling of CCN- and INP-relevant aerosol parameters

R. E. Mamouri and
A. Ansmann

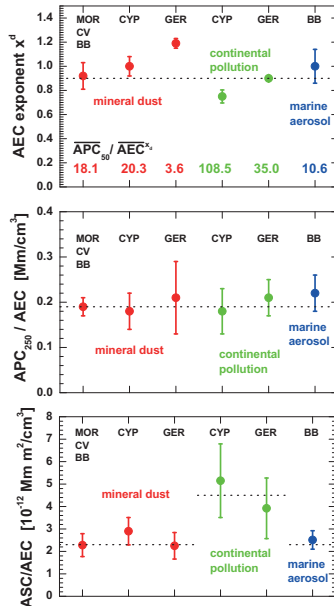


Figure 7. Overview of derived values for the extinction exponent x_i (top panel, required to compute APC_{50} with Eq. 1), $c_{\text{P}250,i}$ (center, required to compute APC_{250} with Eq. 2), and $c_{\text{PS},i}$ (bottom, required to compute ASC with Eq. 3) for 532 nm and the different AERONET data sets listed in Table 3. $c_{\text{P}50,i}$ values (in cm^{-3} at 1 Mm^{-1} AEC, required to solve Eq. 1) are given as numbers at the bottom of the top panel. Error bars (one standard deviation) indicate the uncertainties in the derived parameters. The dotted lines indicate mean values for the different aerosol types (dust, anthropogenic, marine). MOR, CV, BB indicate SAMUM/SALTRACE dust observations, GER Leipzig, CYP Limassol measurements, and BB denotes the Barbados Ragged Point 2007–2015 long-term observations.

Lidar profiling of CCN- and INP-relevant aerosol parameters

R. E. Mamouri and
A. Ansmann

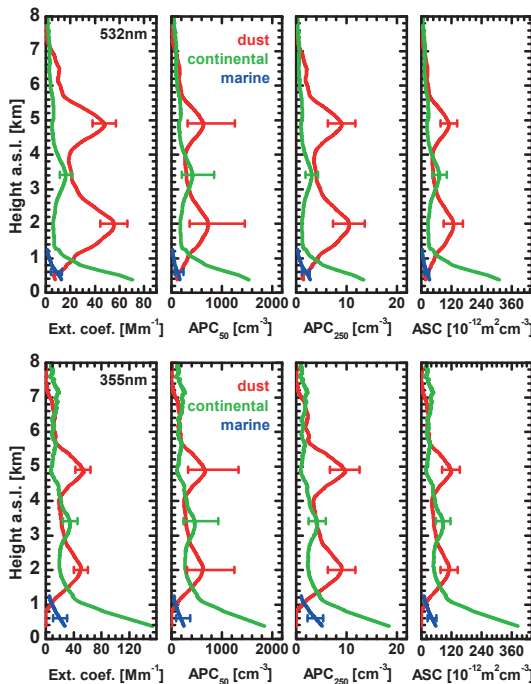


Figure 8. (Top) Height profiles of the 532 nm aerosol extinction coefficient AEC (as shown in Fig. 2), and the derived profiles for APC₅₀, APC₂₅₀, and ASC. The BACCHUS lidar observation was taken with Polly^{XT} at Nicosia on 7 April 2015 during a major dust outbreak from the Sahara. (Bottom) Same plots for 355 nm. The APC₅₀, APC₂₅₀, and ASC profiles from 355 nm AEC differ only slightly from the ones obtained from the 532 nm extinction profiles in the free troposphere, and demonstrate that ESA's space lidars, which will operate at 355 nm, can provide information of the basic cloud-relevant aerosol microphysical properties. Error bars show typical overall retrieval uncertainties.

[Title Page](#)

[Abstract](#)

[Introduction](#)

[Conclusions](#)

[References](#)

[Tables](#)

[Figures](#)

◀

▶

[Back](#)

[Close](#)

[Full Screen / Esc](#)

[Printer-friendly Version](#)

[Interactive Discussion](#)

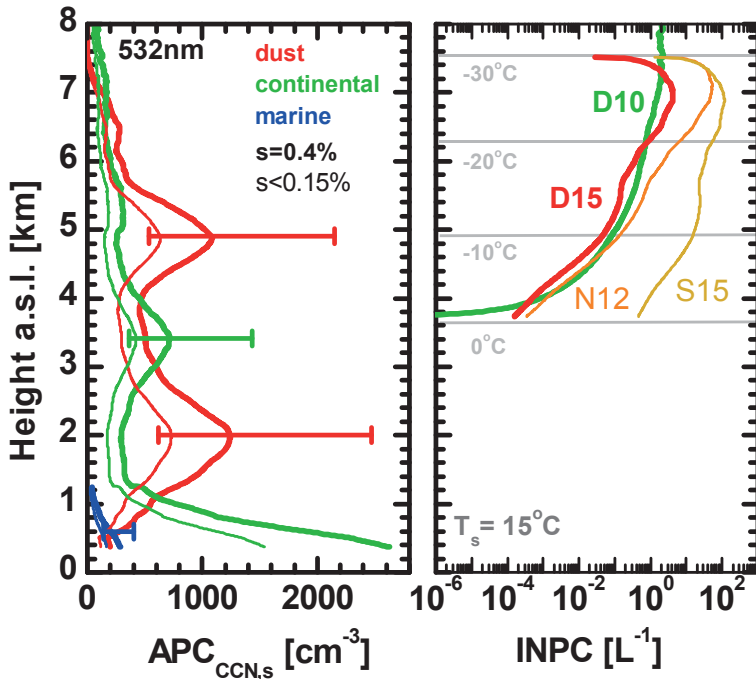


Figure 9. (Left) $APC_{CCN,s=0.15\%}$ (thin red line, Eq. 4) and $APC_{CCN,s=0.4\%}$ (thick red line, Eq. 6), and (right) the derived INPC profiles, computed with the parameterization schemes after DeMott et al. (2010) (D10, Eq. 7), DeMott et al. (2015) (D15, Eq. 8), Niemand et al. (2012) (N12, Eq. 10, immersion freezing), and Steinke et al. (2015) (Eq. 13, deposition freezing). The respective particle input parameters, APC_{250} and ASC, are shown in Fig. 8. Error bars (left panel) indicate the estimated uncertainties (factor of 2). INPC errors are estimated to be within a factor of 2–5. T_s is the surface temperature.

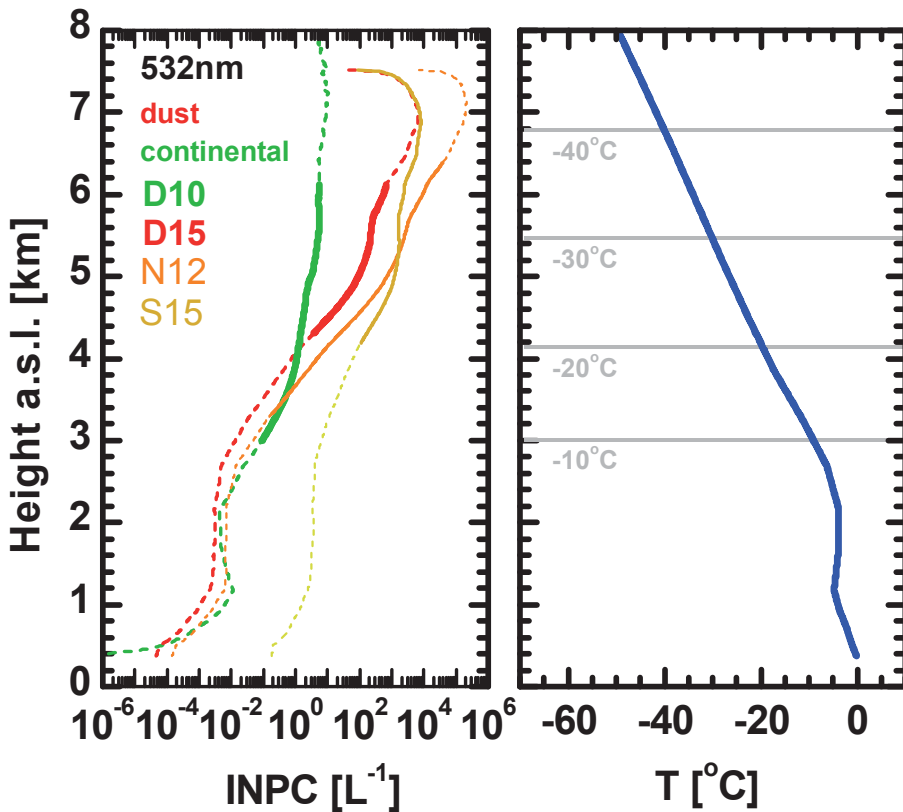
Lidar profiling of CCN- and INP-relevant aerosol parametersR. E. Mamouri and
A. Ansmann

Figure 10. Profiles of INPC after shifting the entire GDAS temperature profile by about 15 K towards lower temperatures so that the surface temperature is 0 °C. Thick solid line segments in the left panel show the temperature ranges for which the different parameterizations are derived and thus fully applicable.

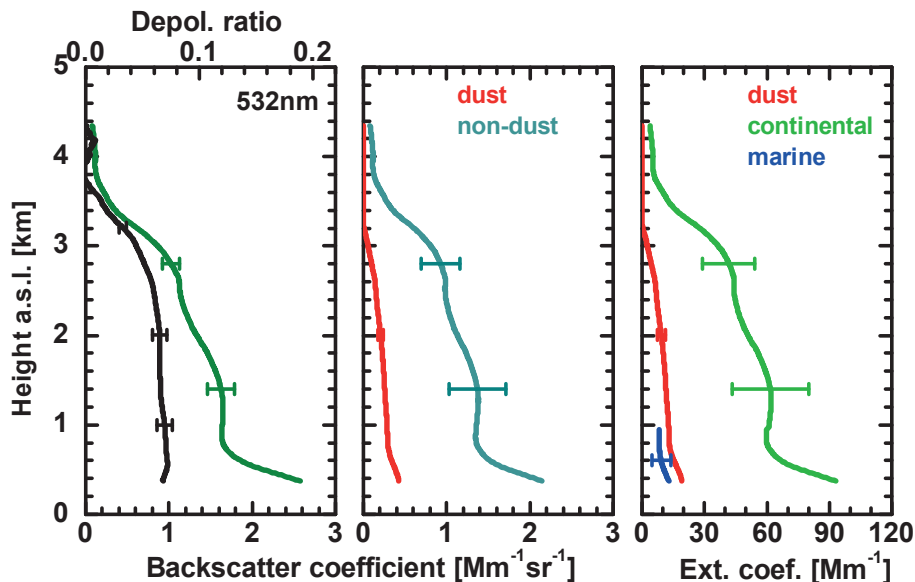
Lidar profiling of CCN- and INP-relevant aerosol parametersR. E. Mamouri and
A. Ansmann

Figure 11. Same as Fig. 2, except for a lidar observation at Limassol on 16 August 2012. On this day, continental aerosol pollution from Turkey, the Black Sea area, and from southeastern and central Europe was advected to Cyprus at different heights up to 4 km. Lidar ratios used in the conversion of backscatter into extinction profiles were 50–60 sr for continental pollution and 45 sr for mineral dust.

Lidar profiling of CCN- and INP-relevant aerosol parameters

R. E. Mamouri and
A. Ansmann

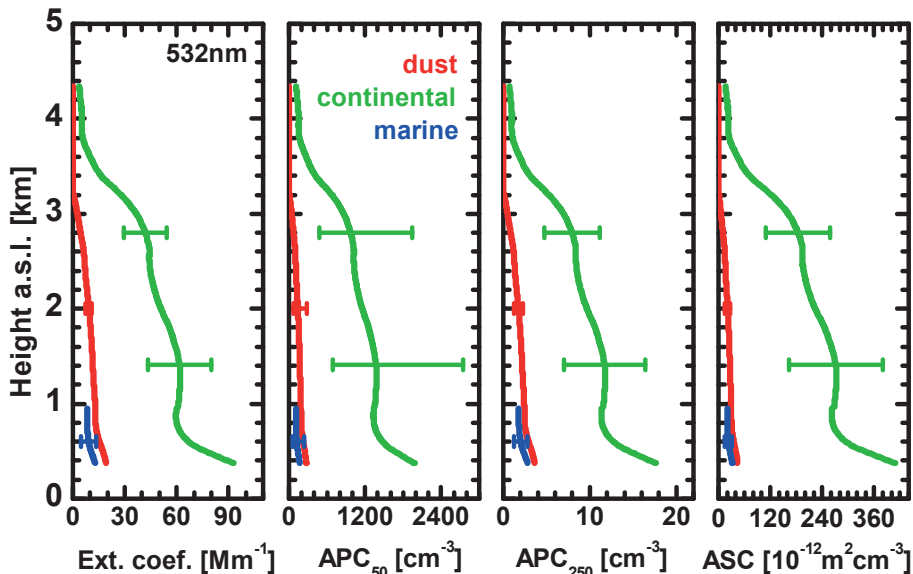


Figure 12. Same as Fig. 8, except for the lidar observation of aged anthropogenic aerosol on 16 August 2012 shown in Fig. 11.